LUT UNIVERSITY
LUT School of Energy Systems
Mechatronic System Design

Ivan Kulagin

DESIGN OF ROBOTIC HORSE HEAD AND NECK MECHANISM

Examiners: Professor Heikki Handroos
Post-doctoral researcher Ming Li

ABSTRACT

LUT University
LUT School of Energy Systems
LUT Mechanical Engineering

Ivan Kulagin

DESIGN OF ROBOTIC HORSE HEAD AND NECK MECHANISM

Master's thesis

2020

77 pages, 63 figures, 10 table

Examiners: Professor Heikki Handroos
Post-doctoral researcher Ming Li

Keywords: horse riding simulator, horse motion, mechanical optimization, power optimization

This work is part of horse-riding simulator development project carried out in Laboratory of Intelligent Machines in LUT University.

The work is aimed to develop horse simulator head and neck mechanism that could realistically imitate horse motion. Following development steps are discussed in this work: horse head and neck motion analysis for walk, canter and trot gaits; kinematics synthesis; analysis of mechanism dynamics; optimization of mechanism power consumption; mechanical design including CAD modeling, cost-saving and manufacturing optimization. The outcome of the work is the CAD model of horse head and neck mechanism that can reproduce desired horse motion patterns.

ACKNOWLEDGEMENTS

I would like to express my deep and sincere gratitude to my supervisors, Professor Heikki Handroos and Post-doctoral researcher Ming Li who gave me the opportunity to work and study in the Laboratory of Intelligent Machines, gave freedom of choice in decision making and provided constant guidance during the research. I also would like to acknowledge Dr. of Science Sergey Kolyubin, my supervisor in ITMO university.

Ivan Kulagin

Ivan Kulagin

Lappeenranta 13.05.2020

TABLE OF CONTENTS

LIST OF SYMBOLS AND ABBREVIATIONS

CAD	Computer-aided design
FDM	Fused deposition modeling
FEM	Finite element method
Mocap	Motion capture
RPM	Revolution per minute

1 INTRODUCTION

Simulator is a powerful tool that can help someone to prepare for a dangerous situation or for a situation where any mistake would have an enormous price. Furthermore, simulators can bring someone a new experience that otherwise would be hard or impossible to get. Horse-riding simulator covers both areas, it can help a beginner rider to get used to the new activity as well as the simulator can give someone a new interesting experience who has no opportunity to ride a real horse. Currently there is a demand for such simulators which can easily be explained.

First of all, a beginner rider needs many hours training every day. A rider is capable of doing that whereas a horse can be exhausted after an hour of intensive training. That is why horses are changed quite often. This is an expensive activity and replacing several horses with one riding simulator could drastically reduce costs of rider trainings.

Second but not less significant point, inexperienced rider can squeeze horse sides too much while giving a command for a horse using legs or for the same reason a rider can pull a harness with too much force. In these and many other situations beginning rider can harm a horse or in some other cases lack of experience can cause serious damage to a rider. On the contrary, a rider using a simulator is not able to harm any animal and the chance of injuries caused by a simulator practically equals to zero.

Nowadays there are several companies in the world which provide professional horse-riding simulators, but all of them have at least one major drawback. This drawback is horse head and neck do not have any motion at all or in more advanced simulators these parts move but not realistically since designs are usually based on cost-effectiveness of manufacturing without taking in account accuracy of motion. Realistic motion of horse head and neck is essential for a rider in order to develop riding skills since arms of a rider should be perfectly synchronized with horse head motion. That is why development of a horse-riding simulator that would include a realistic horse head and neck mechanism is important.

Aim of this work is to develop such a mechanism that would realistically reproduce horse head and neck motion with cost-effectiveness and ease of manufacturing taken in account. During the work process will be considered design matters that will include: horse motion analysis and creation of trajectories that mechanism will reproduce; trajectories will be obtained based on different sources in order to be compared and validated; several kinematic schemes will be considered, for each scheme dynamical simulation will be carried out what will allow to chose the most suitable scheme; lastly, the desired mechanism will be modeled in CAD (Computer-aided design) software and this process will go along with the dynamical analysis and optimization. As the result fully functional CAD model of horse head and neck mechanism will be presented.

1.1 Literature review

Many publications on the topic of horse movement have been considered, and one of the most important is work of Bhatti, Shah & Shahidi (2013, p. 139) which shows that "a procedural model has been developed for synthesizing cyclic horse motion through trigonometric functions. The system has been developed and implemented using mathematical model derived from trigonometric cyclic equations, along with forward and inverse kinematics to produce absolute gait control over the locomotion of horse character". Horse skeleton during motion with different gaits is visualized frame by frame. It gives good understanding on how skeleton should move.

Paper written by Loscher, Meyer, Kracht & Nyakatura (2016) gives understanding of why horses and other ungulates move heads during locomotion. In this work movement of eight horses during walk gait were analyzed. The output of the research is dependency of horse heads and withers height and acceleration versus stride duration. The work states that examined parts during walk oscillate with a phase shift of 25% of the stride cycle duration.

A few other publications contain information about horse body dimensions. Padilha, Andrade, Fonseca, Godoi, Almeida & Ferreira (2017) defined average values for all necessary horse body dimensions, which are shown in table 1.

Table 1. Individual linear measurements, means, standard deviations, and medians of Brazilian Sport Horses undergoing training for eventing. (Padilha et al. 2017)

	Mean (*m*)	Standart deviation (*m*)	Median (*m*)
Withers height	1,62	0.034	1,62
Croup height	1,63	0.039	1,62
Body length	1,6	0.062	1.61
Croup length	0.52	0.026	0.51
Shoulder length	0.53	0.022	0.53
Neck length	0.68	0.042	0.68
Head length	0.63	0.021	0.63
Head width	0.22	0.012	0.22
Chest width	0.42	0.018	0.42
Hip width	0.54	0.018	0.55
Distance from the elbow to the ground	0.92	0.03	0.93
Distance from the sternum to the ground (empty substernal)	0.86	0.019	0.86

Beside publications, existing solutions and companies are also needed to be analyzed. One of the lead companies in manufacturing of horse simulators is Racewood Ltd. Their main product has several variations; however, concept remains the same. The product is a horse body which is based on a platform with several degrees of freedom, shown in figure 1.

Figure 1. Racewood horse-riding simulator (Racewood Ltd. 2020).

The product also includes horse head and neck mechanism which has two revolution degrees of freedom that is attached to the body. First joint of the mechanism is located at the junction of body and neck and the second joint is located at the junction of neck and head. The company owns (Pat. US 7749088B2 2010), but this patent only describes horse body excluding any information regarding head or neck.

Some other companies provide solutions that are focused on entertaining instead of simulating. As their products are quite similar only one will be discussed, that is “VR Horse” developed by Guangzhou Steki Amusement Equipment Co., Ltd (figure 2).

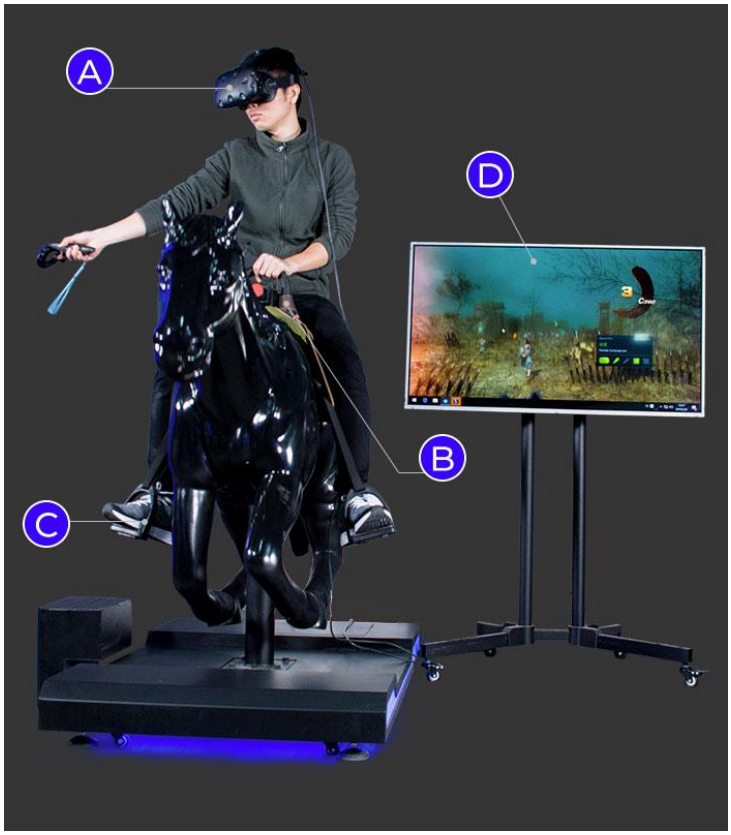

Figure 2. VR Horse (Guangzhou Steki Amusement Equipment Co., Ltd 2020)**.**

This solution consists of one-piece body which is attached to a rack fixed to the ground. Relative to the rack the body has two degrees of freedom in vertical plane. The body does not have proportions of a real horse, yet the realism effect is achieved by using VR device. Similar concept with more realistic horse body is also provided by Racewood Ltd. Although use of VR provides good visual immerse experience, it cannot provide feeling of moving harness which rider is always in contact with.

Another major question is to design a mechanism that would be able to reproduce a desired horse head and neck trajectories. One possible solution is to use algorithm to create a necessary mechanism automatically. Example of such an algorithm is described in article by Ha, Coros, Alspach, Bern, Kim & Yamane (2018). The publication presents an approach to designing robotic devices that use serial kinematics from high-level motion specifications. The designed software can define a set of possible kinematic structures based on a library of modular components and user needs to define a set of input trajectories that specify how an end effectors and bodies should move. Although this is a fast way to achieve mechanism that can reproduce a desired trajectory accurately, such an algorithm can only offer serial kinematic design that is not optimized for serial or mass production. Thus, use of this algorithm may cause extra costs as a mechanism designed manually would be more optimized from a cost-effective point of view.

Several software packages already exist that can perform mechanism synthesis and optimization. Examples of these programs are “GIM Software” by COMPMECH Research Group and “SAM Mechanism design” by Artas Engineering Software. The first mentioned software has less functionality. The advantage of the second software is ability to carry out optimization using multiple parameters such as trajectory of a node, any motion or force quantity, geometry of mechanism, mass, spring constant, transmission ratio and others. The software considers not only kinematics but also dynamics, all that makes it an advanced tool for mechanisms designing. However, a license for using this software is needed, which is quite expensive in terms of use in a single case. That is why other methods of mechanisms synthesis should also be considered.

From perspective of motion analysis, software with free license usually have less functionality. However, GeoGebra is mathematics software with wide variety of tools that could be very handy for kinematics design and analysis stage. GeoGebra gives opportunity for fast geometric modeling of almost every possible plane mechanism. Included tools make it easy to measure and manually adjust mechanisms’ parameters.

The project requires manufacturing of realistic stretchable skin imitation that would cover horse neck. The necessity for that is caused by high neck flexibility what makes impossible to use solid bodies to cover the neck (Pat. US 20110087354A1 2016) describes a

technological process of realistic skin manufacturing. The process consists of several major steps: desired surface scanning; preparation of internal components of a machine, they need to be covered so that during pouring process no liquid would get inside; manufacturing of external mold; and the pouring process itself. The advantage of the method is high integration of skin and a mechanism which brings high durability. Precise copy of a desired surface can be reached with use of 3D scanning and accurate mold manufacturing. And finally, this method also brings decent dust and moisture resistance. The drawback of the method is its cost which may be unreasonably high in this case.

Another way of skin implementation is stretching a sheet of flexible material around a frame. In order to make experience of interacting with horse realistic a proper material must be chosen. Publication by Cabibihan, Pattofatto, Jomaa, Benallal & Carrozza (2009) compares several materials with a human skin. Although this project requires animal skin implementation, a horse rider for example will not often directly touch a horse simulator neck and it is important to focus on horse neck appearance, so the results of publication can be used in this case. The publication compares several materials properties with human skin and according to the outcome all investigated the materials could not reach the same properties human skin has. But silicone properties turned out to be the closest to real skin especially its deflection properties. Thus, silicone should be considered into as material for the horse simulator neck.

2 METHODS

The project is based on theoretical studies, no physical experiments were carried out before construction of the first prototype. In order to be sure that the mechanism will be as accurate and efficient as possible several different data sources have been used for identifying horse moving patterns, one for creating trajectories and other for validation. To find the most efficient solution two different mechanism were analyzed and compared, each of them has different modifications aimed to optimize the design. As mechanisms have the same accuracy, they were compared for energy efficiency and cost efficiency.

2.1 Horse gaits analysis

First of all, it was necessary to understand how a horse moves its head during different gaits. According to paper by Bhatti et al. (2013) horse skeleton motion was simulated for walk, trot and canter. This resulted in sets of horse skeleton images that illustrate horse motion in time. An example of such a set for trot motion is shown in figure 3.

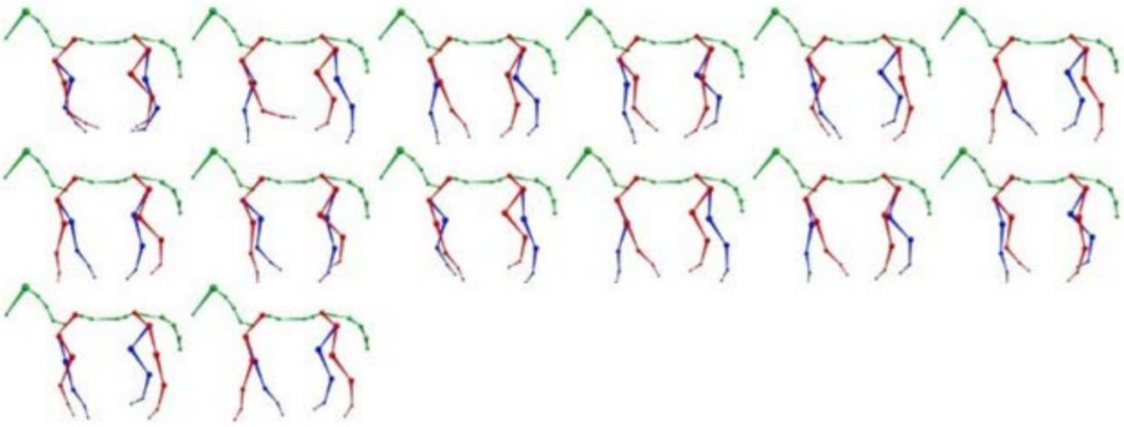

Figure 3. Procedural Model of Horse Simulation (Bhatti et al. 2013).

It was decided that horse must reproduce walk, trot and canter gaits. The paper has all the necessary gaits and they have clear representations frame by frame. These makes interpreting of the results a very easy and fast process in comparison to motion capture analysis. Although motion capture data could provide more accurate dimensions it is not necessary to accurately reproduce a certain horse, instead it is needed to accurately reproduce a horse motion pattern.

That is why the motion study is based on the Procedural Model of Horse Simulation research and motion capture is not considered as the main data source.

In order to build head and neck trajectories every critical point was marked on the skeleton illustrations. The points of interest are “Neck, middle”, “Neck, top”, “Head” and “Nose”. Also, on every frame “Neck base” point was marked which was used later during a process of combining points. In figure 4 is shown an example of marking “Head” and “Neck, top” points for walk gait.

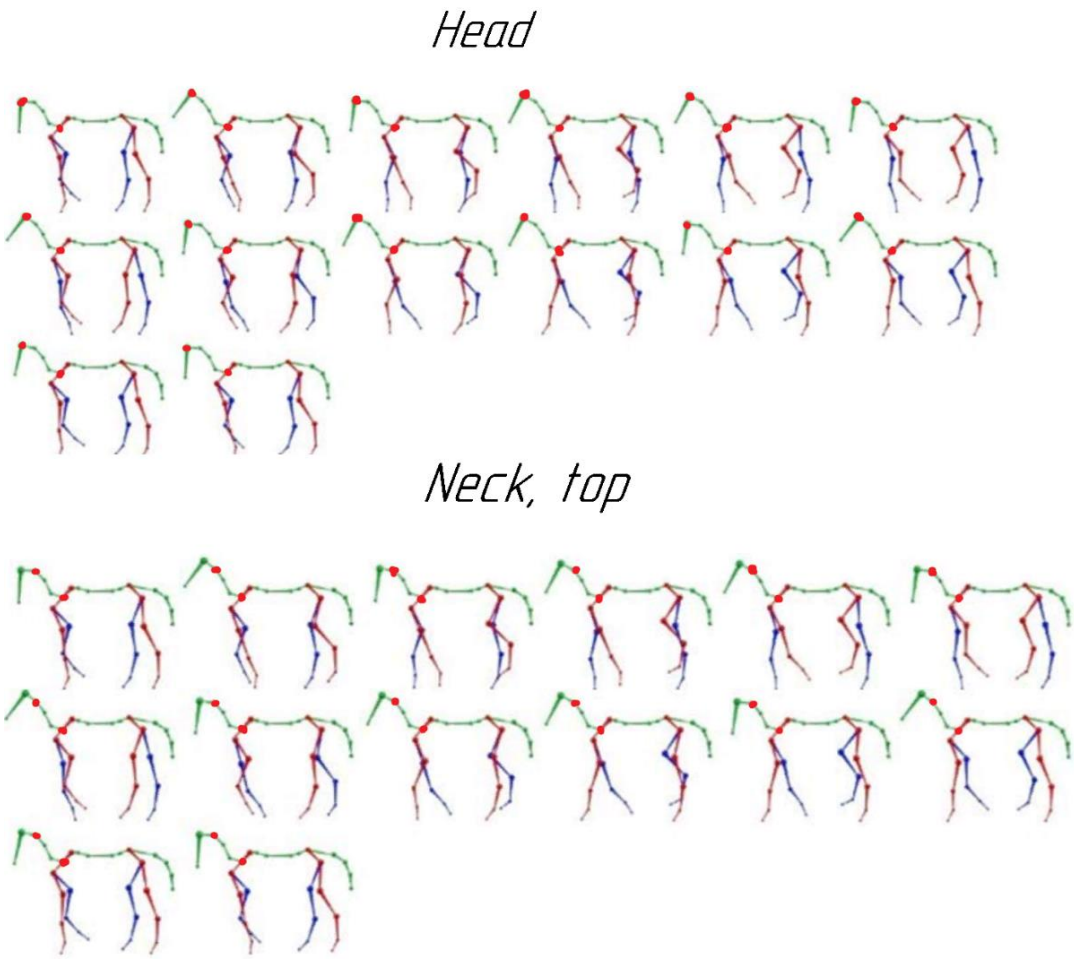

Figure 4. Example of marking critical points (marked with red color) for walk gait. Illustration adopted from Procedural Model of Horse Simulation (Bhatti et al. 2013).

The same procedure was applied for every critical point of each gait. Then all the points related to a certain part of the body and to a certain gait were combined. “Neck base” point which was presented on all frames served as a reference point.

Every group of points were connected by splines and these splines are considered to represent trajectories of motion of certain parts of horse body. An example of obtained trajectory for the “Head” point for walk gait is shown in figure 5.

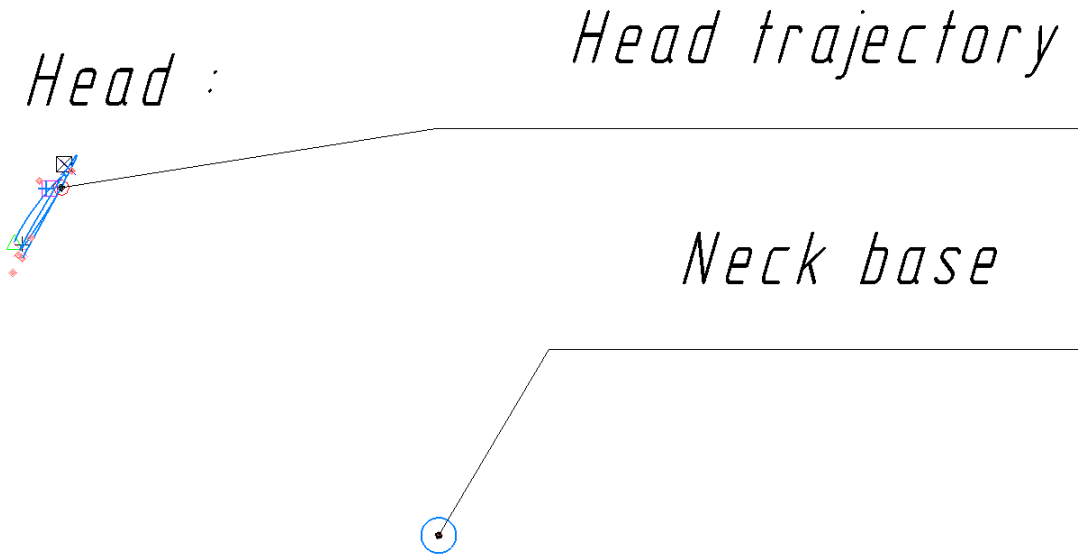

Figure 5. Trajectory of horse head for walk gait.

Blue curve in the figure above represent horse head motion pattern during walk. Curves for each gait and for each body part were obtained in the same way, thus, there are four considered parts and three gaits and as a result 12 motion trajectories.

Trajectories were combined by type of gait to allow analysis of a certain gait pattern as a whole. This will allow to define range of motion for each gait. Obtained motion trajectories for walk gait is shown in figure 4.

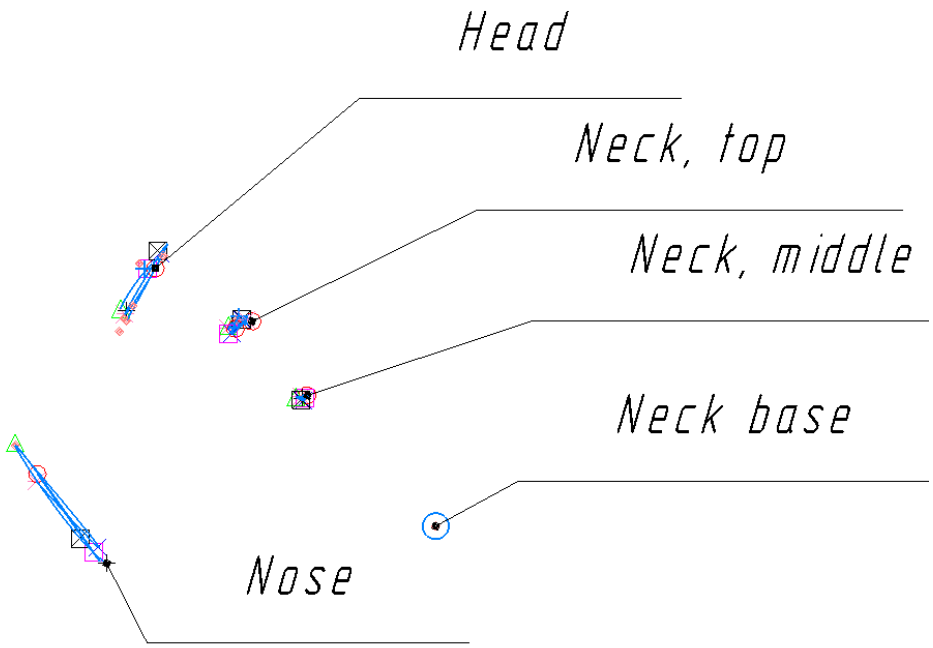

Figure 6. Motion trajectories for walk gait.

It can be seen from the picture that it contains an empty space between “Neck, middle” and “Neck, base”. Initially it was considered to include the fifth point “Neck, bottom”, however it turned out that amplitude of motion neglectable small, thus, the point was excluded from the analysis. “Neck, middle” trajectory also has a small amplitude. However, it cannot be excluded since that will lead to significant reduction of accuracy as on the further steps new splines will be created across trajectory edge points.

Trajectories of all gaits were combined, so they could be easily compared to each other. Furthermore, this will allow to define maximal needed range of motion that horse head and neck mechanism must reproduce.

Trajectories of all obtained horse gaits are shown in figure 7. Each gait is matched with a color: trot – green, canter – blue, walk – black.

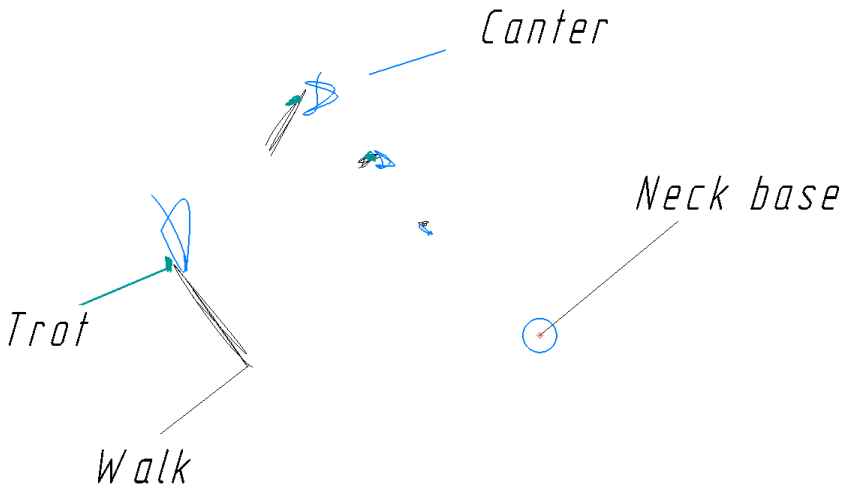

Figure 7. Horse gaits combined.

According to the results trot has the least amplitude and walk has the highest amplitude. Motion range is limited between walk trajectory lowest position and canter trajectory highest position. Neck trajectories are similar for all gaits and the trajectories derivate starts from head.

To look more carefully how horse neck deforms, extra splines were added. These splines pass through edge points of horse body parts. An example of adding extra splines for canter is shown in figure 8.

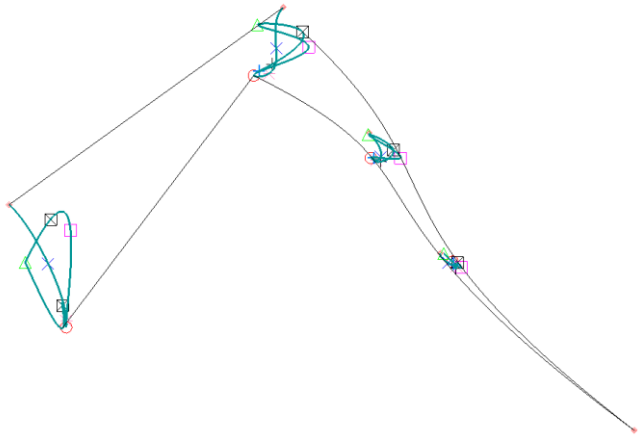

Figure 8. Horse neck deformation during canter.

Horse neck forms an S-shape curve during motion and Horse “Head” and “Nose” points are connected with a straight line and represent horse skull motion. The same actions were made

for other gaits and it turned out that they form similar patterns. Thus, this specific flexibility must be taken in account as the mechanism must be able to recreate similar patterns.

Before doing any further steps, the results must be validated since they are based only on one source. To check the results motion capture data was used. The data was purchased from an outside company and it contains video recordings of a living horse motion with and without a rider. During the shooting process both horse and rider had sets of sensors on their bodies. After postprocessing data for skeletons positions during motion was obtained which was used in this work to validate the results. The motion capture data of a rider on a horse skeleton is shown in figure 9.

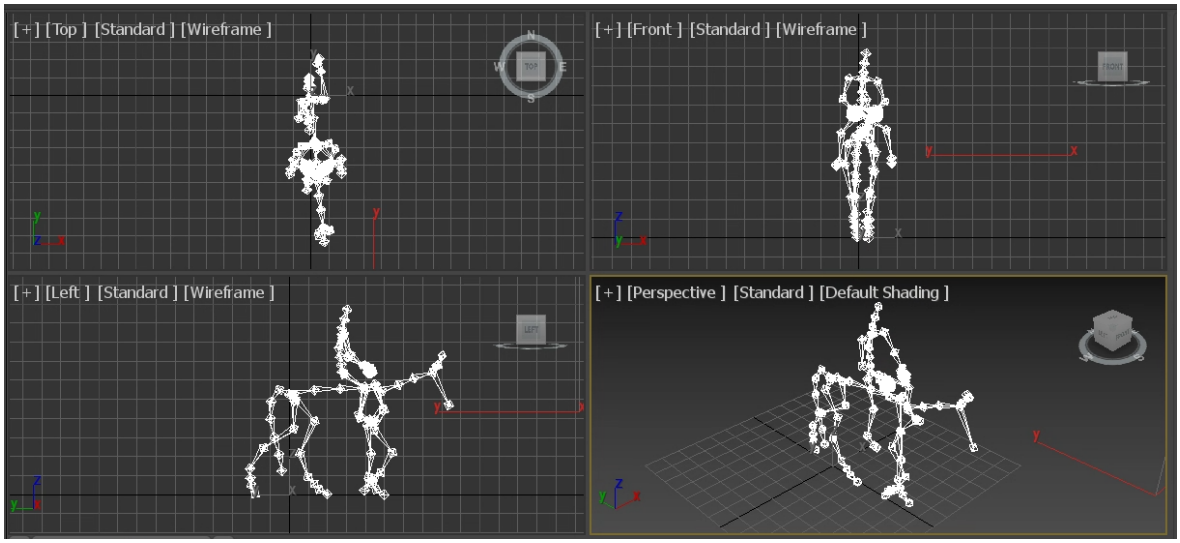

Figure 9. Motion capture data of a rider on a horse skeleton.

Coordinates of each node at any moment of time is given, however used coordinate system has its own scale factor, thus dimensions are different and even though they can be used their recalculation is needed. As with the skeleton coordinate also comes a complete 3D model, it can be used instead to avoid extra recalculations, also in this way method of obtaining trajectories will be similar to the previously reviewed. During the analysis data of a horse with and without rider will be compared to get an understating of how this affects horse head and neck motion trajectories.

Horse motion animation was divided into separate frames and the same critical points were marked. A set of frames of a horse without a rider is shown in figure 8. In the figure “Head”

and “Nose” critical points are marked and other points were not taken into account since if the trajectories would match for these two points the validation could already be considered as a successful.

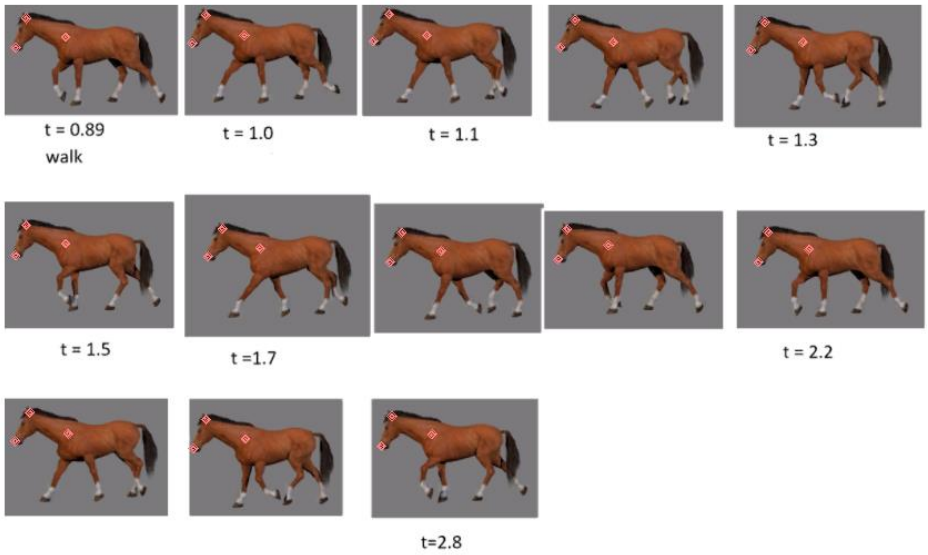

Figure 10. Horse model with marked “Head” and “Nose” critical points.

Time was also measured, so that velocities and accelerations could be obtained. Some difficulties were associated with marking process since this was a horse 3D model instead of skeleton. This problem was solved by defining “Neck base” point as the midpoint of the base of the neck, “Head” point was associated with an ear and “Nose” point with horse nose. This approach of marking does not provide high accuracy, but it is not required. It is only necessary to obtain similar curves to curves that were obtained previously in order to prove that gathered data is valid. The same procedures were done for horse with a rider motion capture data and postprocessed with the same technic as was discussed above. That led to a result shown in figure 9.

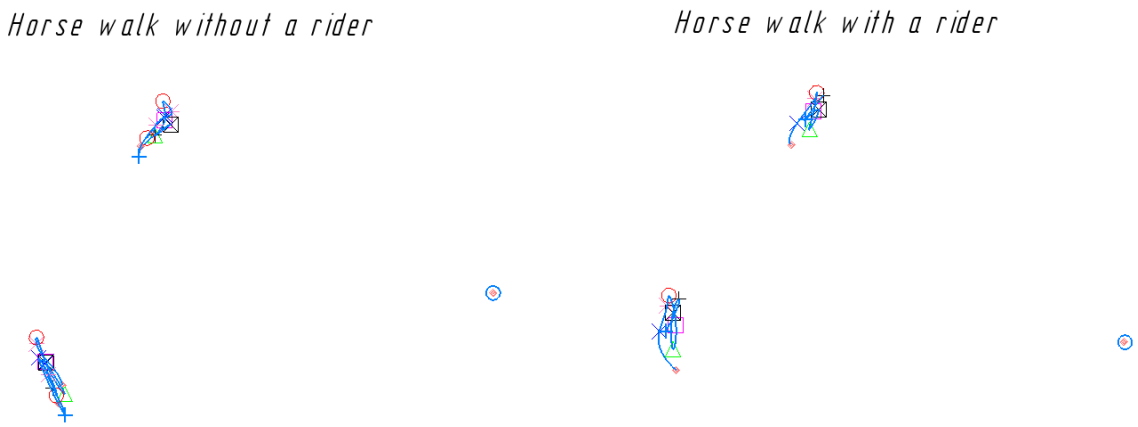

Figure 11. Horse motion trajectories of “Head” and “Nose” points with and without a rider.

These trajectories were combined with walk trajectories that were obtained previously. All curves were brought to the same scale. That was done based on horse skull length, for an average horse the length is 600 mm. Length between “Nose” and “Head” points was considered as a horse skull length and that allowed to scale all sets of trajectories to the same size. All sets were aligned with the respect of “Neck base” point. Comparison between mocap (Motion capture) trajectory sets and trajectories based on simulation is shown in figure 12.

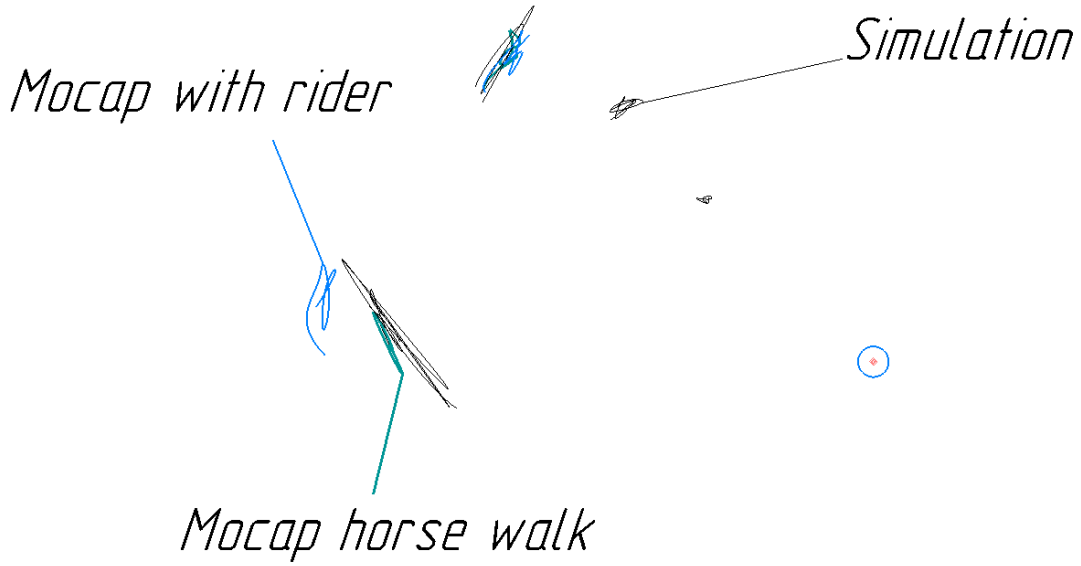

Figure 12. Comparison of trajectories based on mocap and simulation data.

It can be seen from the figure that trajectories have very similar pattern. Thus, it can be concluded that the trajectories are valid, and they can be used for designing the mechanism. It can also be noticed that a horse tends to bend its head more without a rider that should also be taken into account while programming various horse motions.

After the results were checked they can be combined together in order to be used as a reference point in the mechanism design. For this combination splines that represent neck silhouette were added, that is shown in figure 13.

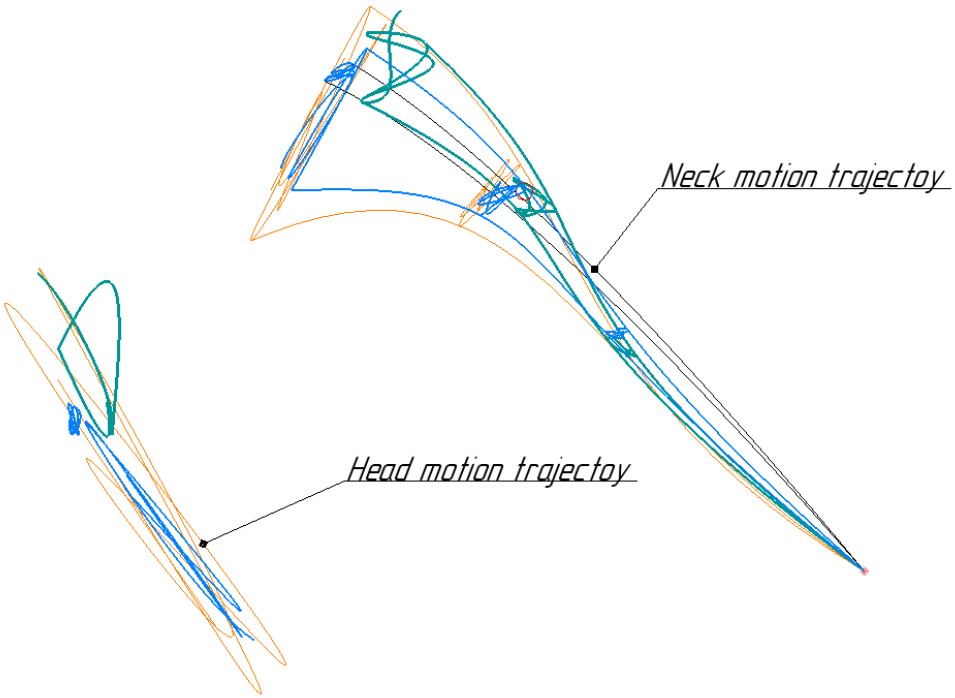

Figure 13. Combine horse head and neck motion trajectories for different gaits.

Analyzing neck motion, it can be noticed that motion amplitude between “Neck base” and “Neck, middle” points is relatively low and will not be visible to a rider. Considering this fact, it was decided to simplify the desired neck trajectory. It had been assumed that the mechanism’s neck would consist of at least two beams and that is why the approximation is made with two lines at the bottom and on the top. The point at which motion of the mechanism starts was shifted closer to head as it will reduce cost without significant loss of accuracy and in this case, mechanism will be shorter, so bending toques values will be smaller.

Desired range of motion for the horse head and neck mechanism is shown in figure 14 and marked with green lines.

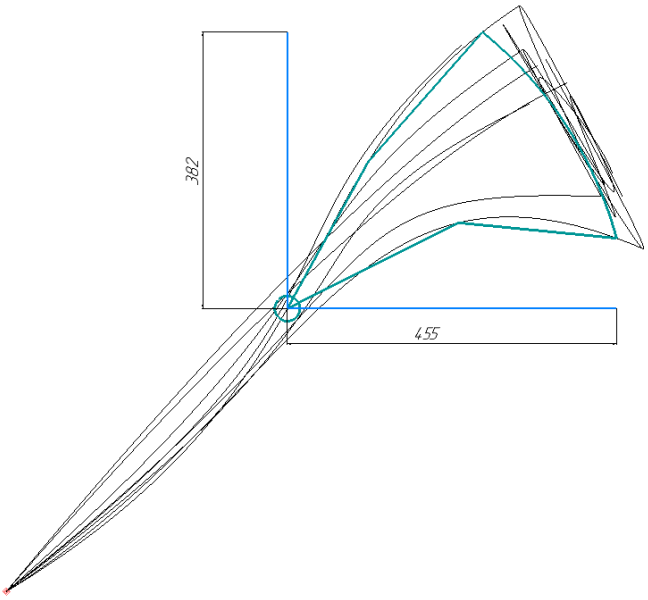

Figure 14. Desired range of motion for the horse head and neck mechanism.

In the figure black lines represent position for different gaits, overall size of the mechanism is defined by blue lines. The last part of horse head and neck motion analysis is defining the maximum range of head rotation. Based on the data collected previously head extreme positions were marked for each gait. The measured extreme angles are shown in figures 15 and 16.

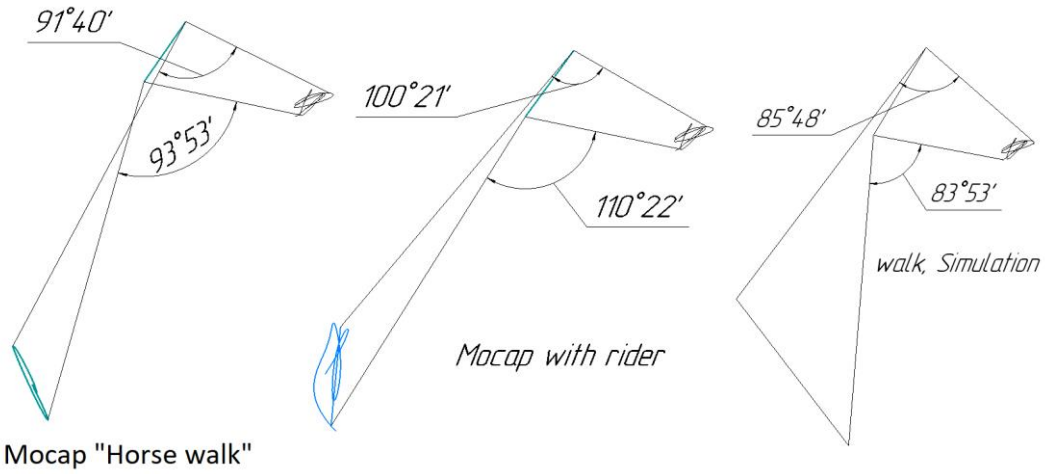

Figure 15. Measurement of extreme angles of rotation of the head based on motion capture and walk simulation.

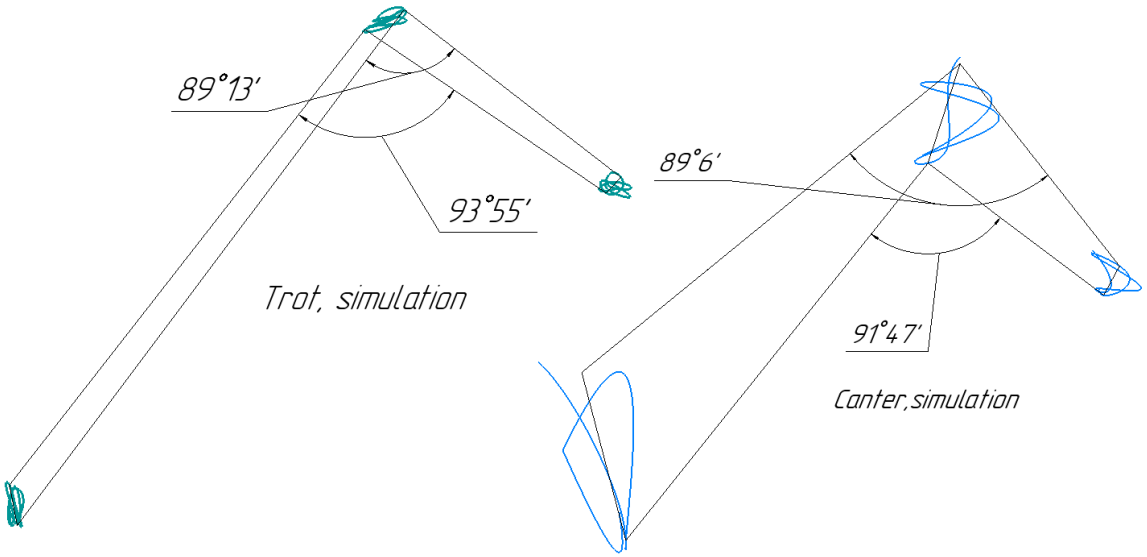

Figure 16. Measurement of extreme angles of rotation of the head based on simulation for trot and canter gaits.

Extreme points of the trajectories were successively connected: “Neck top” trajectory was connected to the “Head” trajectory and then “Head” to “Nose”. Then angles between pairs of lines were measured. As was discussed previously, horse tends to tilt its head more without a rider. The simulator must reproduce both horse behaviors when rider sitting on a horse and a horse moving without a rider. Thus, the inclination angle of horse head with the respect to the horse neck should vary from *80°* to *115°*.

2.2 Kinematics synthesis

The mechanism that will be designed should contain as least number of actuators as possible, in order to reduce cost and dynamic effect on the body. Several variations of lever mechanisms have been proposed so that one with the best performance would be chosen.

In the development process, it is worth starting from the fact that the movement of both parts of the neck, discussed earlier, are interconnected. Thus, it can be assumed that the neck mechanism can be moved by only one actuator, and still it will be possible to reproduce the whole range of desired neck motions. Two additional actuators can be used for rotating head in both vertical and horizontal planes.

Starting from the neck mechanism, a kinematics shown in figure 17 has been proposed firstly.

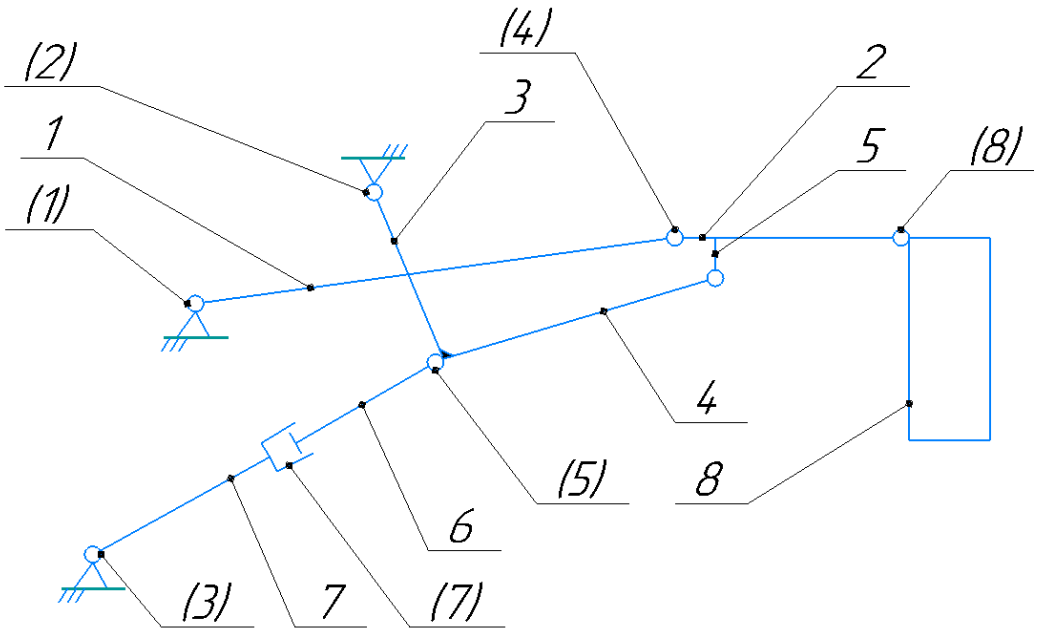

Figure 17. Kinematic scheme of "2-Joint" mechanism.

We will call this mechanism as "2-Joint" since neck connection rod is attached with two revolution joints. Numbers in parentheses define joint and other numbers define links. The construction is driven by a linear actuator which is attached to a horse body. The opposite end of the actuator is attached to an angle beam which is as well connected to a horse body from the one side and to a cantilever beam from another side.

A crankshaft which is attached to a horse body and to the cantilever and the cantilever itself form a horse neck, so a movement of these two elements will reproduce the movement of a horse neck. A horse head will be attached to an end of the cantilever.

Kinematic simulation of the mechanism is shown on the Figure 18. The scheme shows trajectories of two key points "H" and "M" which will define the movement of horse neck mechanism.

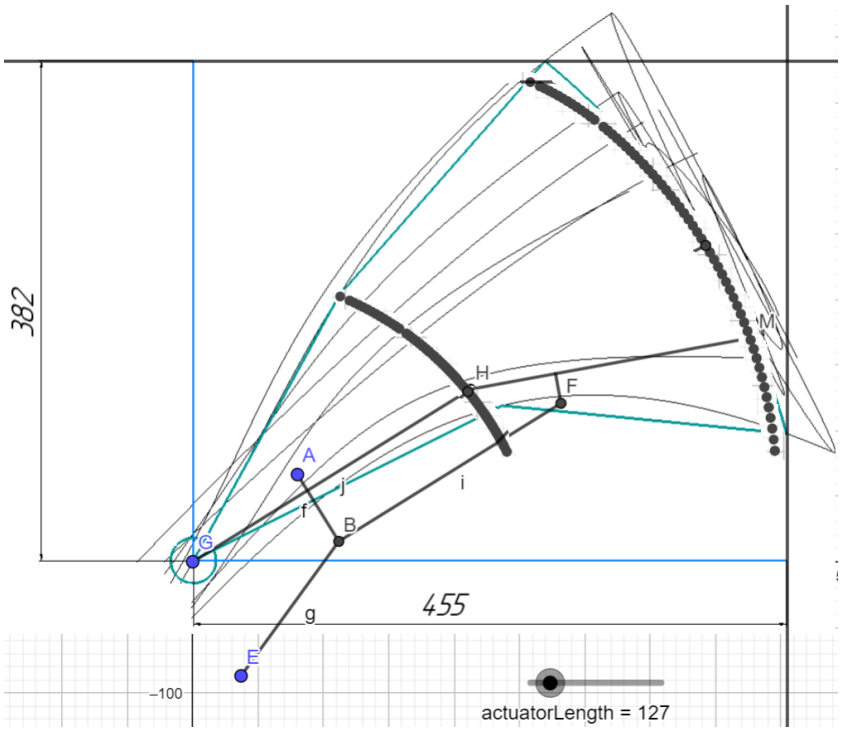

Figure 18. Kinematic simulation of the "2-Joint" mechanism in GeoGebra.

The figure was made with GeoGebra classic and then animated. It can be seen from that the mechanism provides trajectory of the neck which almost completely matches with the desired trajectory achieved on the previous stage.

Points "A", "G", "E" represent revolution joints that are attached to the main simulator frame. "EB" – is a linear actuator which length varies from *118 mm to 180 mm.* Other points represent revolution joints that connect the frame. Point "B" shows two revolution joints combined. Lengths of the beams have been defined manually so that the mechanism could reach the desired trajectory. Length of all beams are shown in table 2.

Table 2. Beams' lengths in "2-Joint" mechanism

EB	*118-180 mm*
AB	*60 mm*
GH	*250 mm*
HM	*220 mm*
BF	*200 mm*
HM-F	*52 mm*

In order to reduce power consumed by the linear actuator the mechanism previously was optimized: point “E” where mechanism is attached to the horse body was repositioned as well as point “A” of a crankshaft “AB”. This led to decrease of required force created by linear actuator, however, this action has a drawback as can be seen from the figure points “A”, “E”, and “G” located close to each other which can bring difficulties during the design of construction process.

In order to fit into neck volume length of the cantilever “HM-F” and crankshaft “AB” have to be reduced, what will also add difficulties during the process of designing. A head which is not shown on the figure will be attached to the end of cantilever “M” and will be driven by a linear actuator.

The second option is “3-Joint” mechanism that is shown in figure 19.

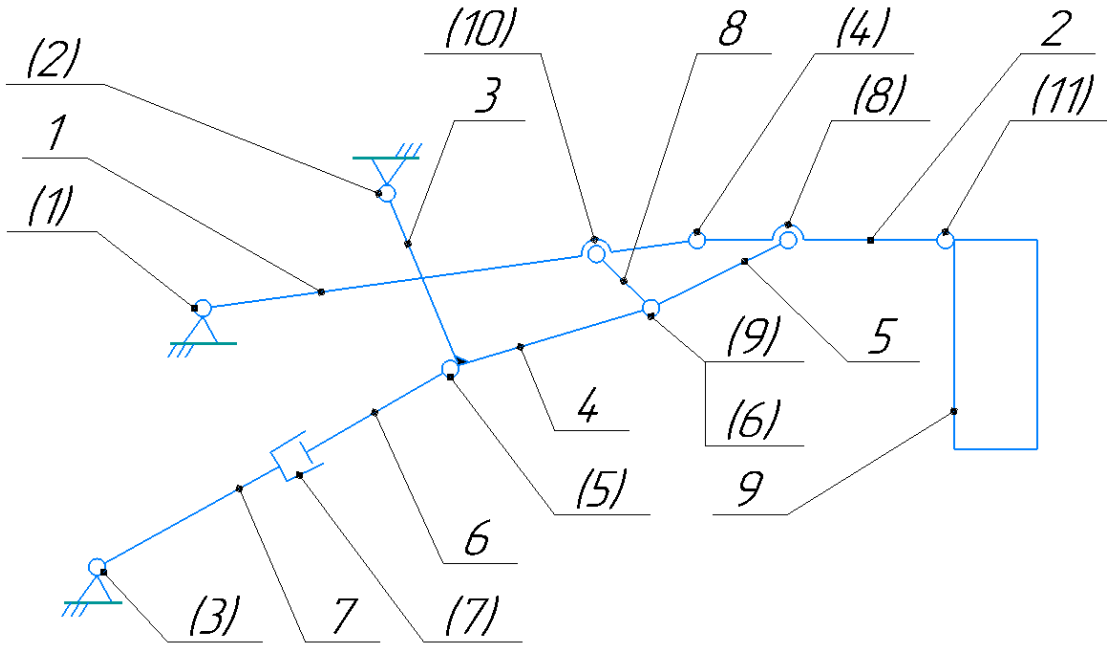

Figure 19. Kinematic scheme of “3-Joint” mechanism.

The mechanism on the figure above is named “3-Joint” because beams that imitate neck are connected with use of three revolution joints. Again, numbers in parentheses represent joints. Similar to previous case, the construction is driven by a linear actuator which is attached to a horse body and the opposite end of the actuator is attached to an angle beam which is as well connected to a horse body from the one side and to a cantilever beam from another side.

The difference between the mechanisms begins from the end of angle beam that has two short connection rods on its right end. Both rods are attached to the angle beam with revolution joints and the opposite ends of each beams connects one of the cervical vertebrae imitating beams.

The difference in constructions is rather small, however, force distribution is different. In case of "2-Joint" mechanism all the force is transmitted from angle beam to the cantilever "HM-F" and the to the beam "HM". And even though this design consists of less components and seems to be more cost effective, it has high force and thus stresses concentration. That does not only overload the beams, but also overloads revolution joints which connect these beams.

In case of "3-Joint" mechanism forces from the angle beam are distributed more equally. As the angle beam has two connection roads, force transmits to the both upper beams decreasing stresses concentration and reducing bending torques.

Kinematic simulation of "3-Joint" mechanism is shown on the Figure 20. The scheme shows trajectories of two key points "J" and "M".

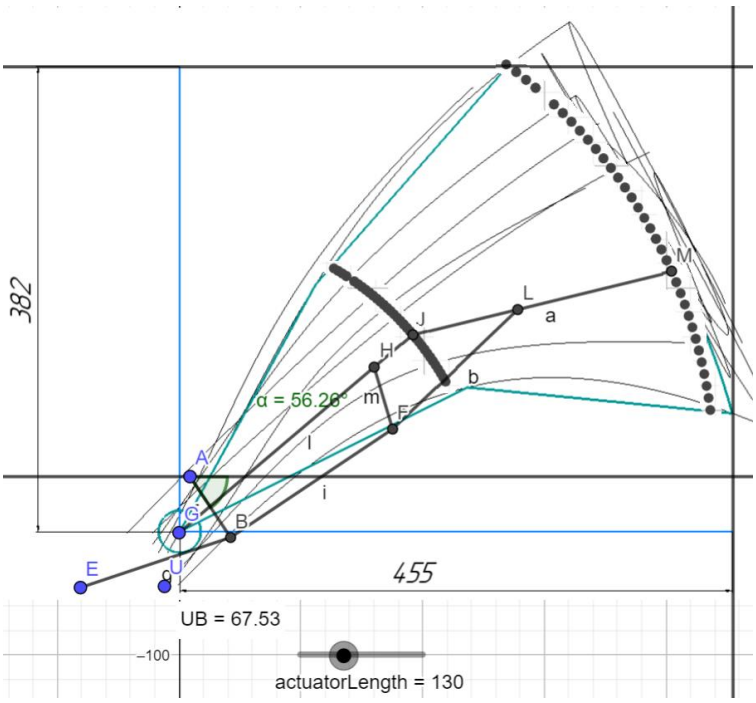

Figure 20. Kinematic simulation of the "3-Joint" mechanism in GeoGebra.

Trajectories left by points “J” and “M” show that the mechanism’s motion range satisfies the desired requirements. Thus, “3-Joint” mechanism can also be potentially used in the simulator. Lengths of the beams in “3-Joint” mechanism are shown in table 3.

Table 3. Beams’ lengths in “3-Joint” mechanism

EB	*118-180 mm*
AB	*60 mm*
GJ	*250 mm*
HJ	*40 mm*
HF	*53 mm*
BF	*160 mm*
FL	*142 mm*
JL	*90 mm*
JM	*220 mm*

2.3 Dynamic analysis

An important part of the development process is a dynamic simulation. To choose one of the proposed mechanisms, their dynamics parameters should be compared. This will help to estimate maximum power consumption what is very important since based on this parameter actuators will be chosen. Also, with use of this, simulation forces acting on the joints and forces acting on the linear actuator can be calculated. The dynamic simulation was carried out in Matlab Simscape.

Parts of both mechanisms were modeled as parallelepipeds with defined masses. Masses were chosen based on assumption that most of the weight will be concentrated in head area, as two actuators will be located there. In simulation head mass was *5 kg.* Masses of beams are varying from *0,2 kg* to *1,0 kg* depending on their lengths.

First, the “2-Joint” mechanism was analyzed, its Simscape model is shown in figure 21. The model also includes actuator for the head, which in case of this simulation is implemented as a rotational motion of a revolution joints. Linear actuator was implemented in a similar way with use of a prismatic joint. For each of the joints desired linear position or a desired angle of rotation is defined and torques and forces in the actuators are calculated based on

this. And as a result, achieved values of critical torques and forces in the actuators can be used to choose suitable actuator models.

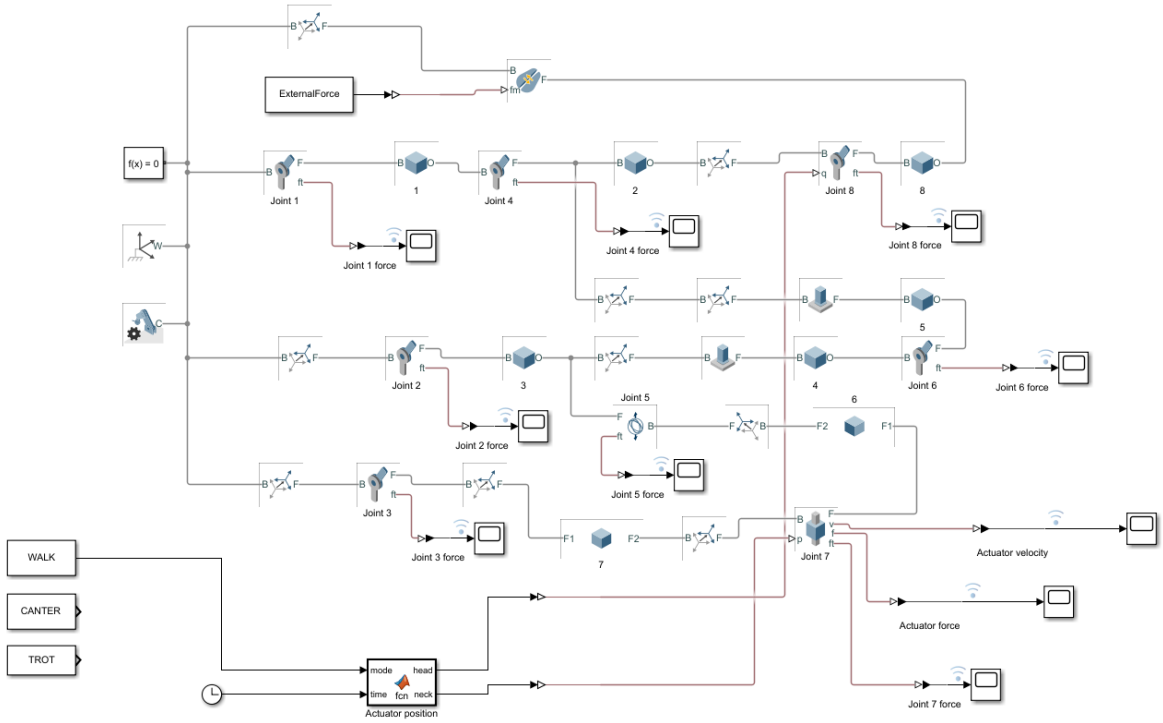

Figure 21. Dynamic simulation model of "2-Joint" mechanism in Simscape.

Based on the data gathered from horse motion analysis it was possible to create an input signal for both actuators and for each horse gait type. As can be seen from the left bottom corner in the figure above the model can be used for simulating different gaits such as walk, trot and canter. To do so a certain data block (which is shown at the left bottom corner) should be attached to an "Actuator position" block. This block sends position signals: desired length of linear actuator and desired angle of rotation for the horse head actuator. The position signals are then converted to a physical signals with the use of "Simulink-PS converter" block. This is required because actuators can only work with physical signals. Forces in the actuated joints are calculated automatically and later this data can be collected.

Both position signals are sinusoidal with equal frequency and different phase and amplitude. In the research by Bhatti et al. (2013) horse motion was modeled with use of harmonic functions. The results of the research were compared with motion capture data and validated

previously in this work. Since the compared results of the modeled harmonic motion and the motion of a real horse are similar it can be concluded that use of harmonic signals is acceptable in the Simscape model.

Another aspect included in the model is extra force provided by a rider that pulls horse harness. A person riding a simulator may have no actual riding experience and can pull with the whole-body mass leaning back on the horse. Due to this pulling force is assumed to be *300 N* at maximum and *100 N* average.

"2-Joint" mechanism during simulation process is shown in figure 22. Brown rectangle on the right represents horse head, brown and green cylinders are linear actuator, angle beam consists of green and blue rectangles and the rest rectangles are cervical vertebrae beams.

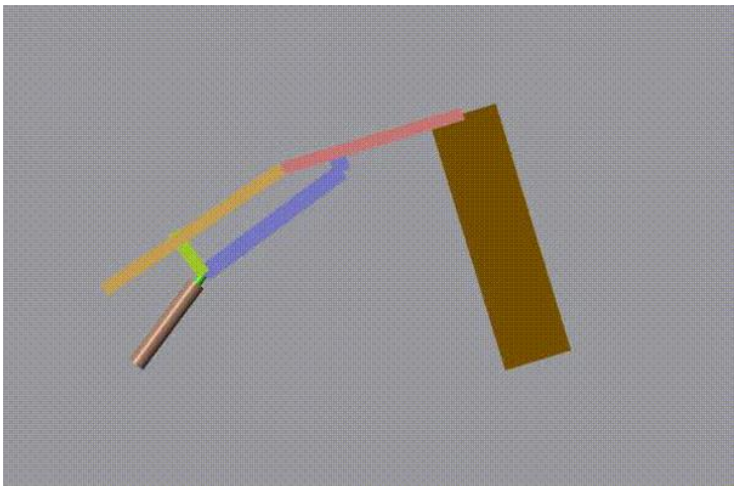

Figure 22. Simscape model of "2-Joint" mechanism during simulation process.

The most important outcome from the simulation is peak values of force generated by the linear actuator and its peak velocity. This is important because the linear actuator consumes most of the power and thus it will be the most expensive part in the mechanism, so first of all the analysis should be focused on this actuator. It is also necessary to compare peak values that existing actuators can reach to make sure that the desired output of the mechanism is

physically possible to reach. The model has been simulated for 5 seconds for each gait. The results of the simulation are shown in table 4**.**

Table 4. "2-Joint" mechanism linear actuator peak values for force and velocity

Gait	Peak force generated by actuator, *N*	Actuator peak velocity, *m/s*
Walk	*1600*	*0,130*
Trot	*630*	*0,025*
Canter	*900*	*0,120*

It can be observed that the walk gait has the highest values therefore it will be examined more thoroughly. Plots of linear actuator generated force and velocity are shown in figure 23.

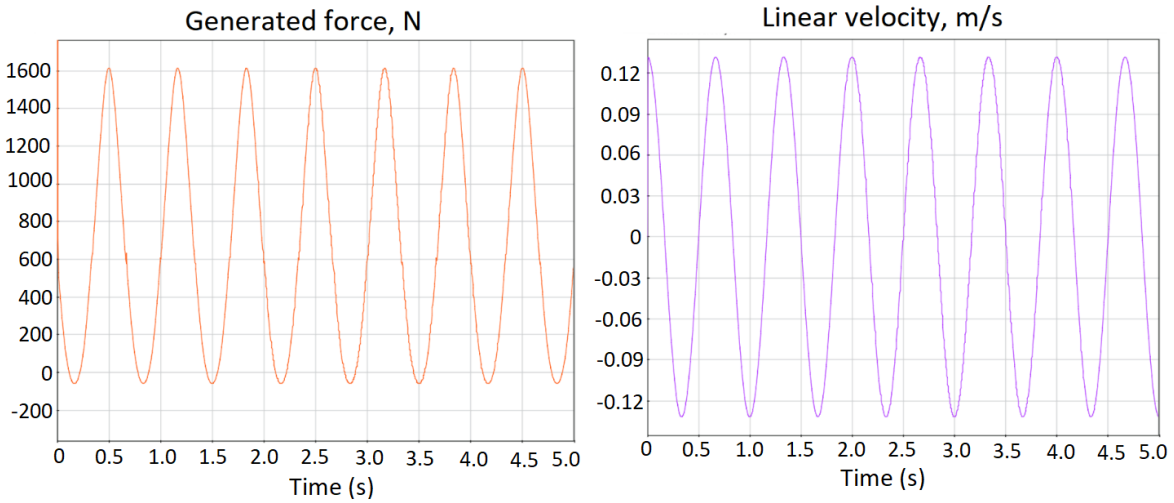

Figure 23. Force generated by linear actuator and its linear velocity for the walk gait in "2-Joint" mechanism.

Simulation shows that force and velocity have the same oscillation frequencies and different amplitudes; of all gaits walk has the highest average and peak power consumption of 180 *W*. At first glance this may seem contradictory, but in fact horse head has much lower amplitude of motion during other gaits and as a consequence accelerations and velocities are lower which leads to lower energy consumption by head and neck. This simulation does not

consider any friction forces or damping as it is difficult at this stage to get valid values for these parameters. Thus, it can be assumed that required power is 10% higher, to have enough capacity to withstand the friction forces.

Collected data shows values of parameters that the linear actuator must have. Search for actuators with required parameters has resulted in several options. However, linear actuators that are capable of generating needed forces are too expensive, average price for such product is higher than *1000 €*. Also, these actuators are too big to fit inside horse neck mechanism. Thus, the mechanism is needed to be optimized, so it would consume less energy and require less power. One option is that energy optimization can be done with the use of a counterweight attached to the beam "G-H" from the left side (figure 18**)**. Next stage of the dynamics analysis is study of forces in joints. These forces were measured during the same *5* second simulation and the outcome of it for walk gait is shown in figure 24. The walk gait is chosen because it is the most loaded gait.

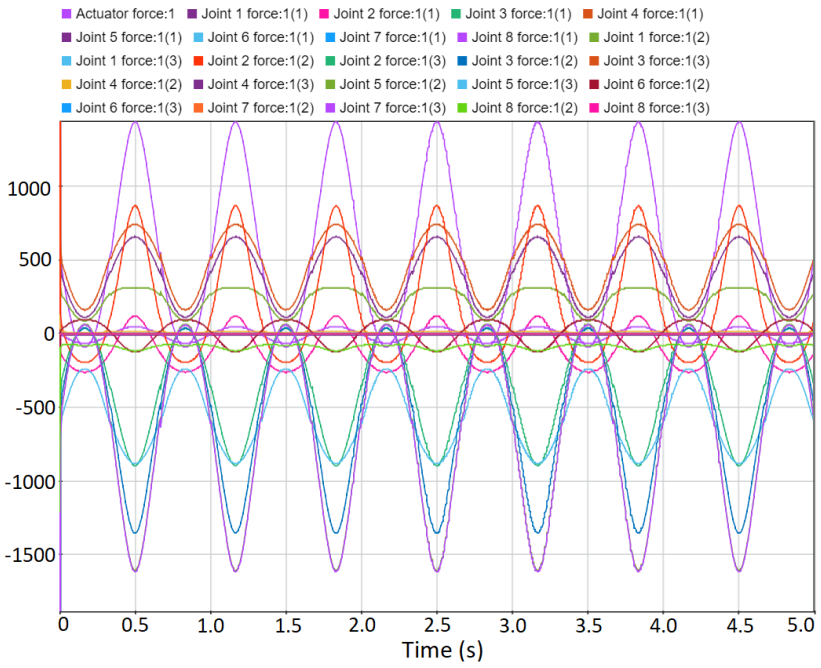

Figure 24. Forces, *N*, in joints during a walk simulation of "2-Joint" mechanism.

It can be seen from the figure above that the joint "G" has the largest amount of forces affecting it which have an upper limit of around 1500 *N*. Joint "A" has also a high amplitude

of forces, but they act in the range from zero to -1000 *N*, whereas forces acting on the "G" joint have alternating amplitude in the range from -1500 *N* to 1500 *N*. That makes this joint extremely vulnerable to fatigue and precautions must be made on the stage of construction design.

Forces in other joints have significantly less amplitude which is also not alternating. This can be considered as an advantage of the mechanism as only one joint requires high attention during the design. Now "3-Joint" mechanism must be considered. A Simscape model of the mechanism is shown in figure 25.

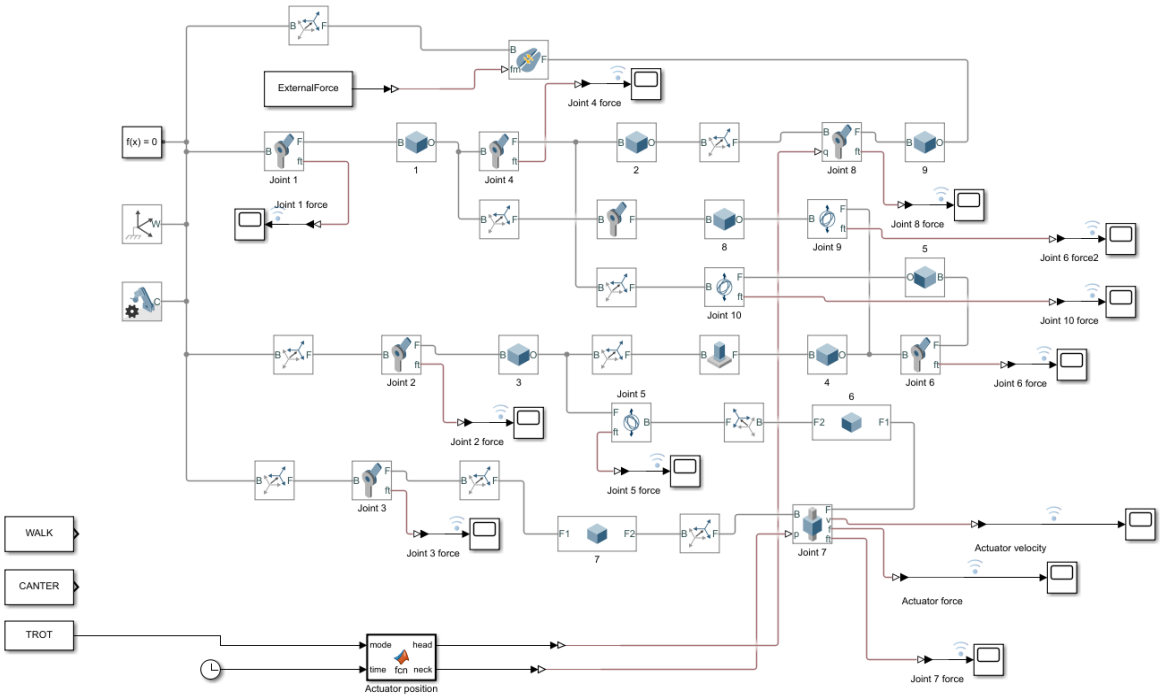

Figure 25. Dynamic simulation model of "3-Joint" mechanism in Simscape.

As like as in the previous case, there is an option of simulating different gait types and an extra force from rider is affecting the mechanism. Comparing Simscape models of the mechanisms, model of "3-Joint" has additional solid block which is connected to the neck crankshaft via bearing joint and to the crankshaft with the linear actuator via revolution joint.

Bearing joint in this case is equal to the revolution joint yet use of two revolution joints would bring unnecessary constrain into the model.

"3-Joint" mechanism during simulation process is shown in figure 26. The model consists of nine rigid bodies most of which are interconnected with revolution joints. One prismatic joint is used to simulate the linear actuator.

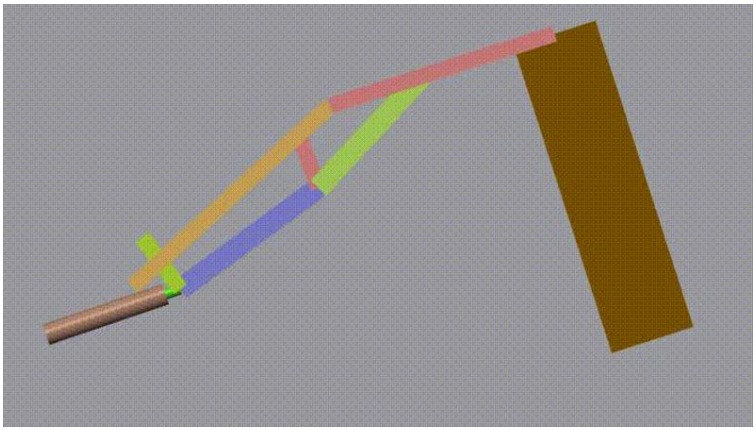

Figure 26. Simscape model of "3-Joint" mechanism during simulation process.

The same simulation procedure was carried out for "3-Joint" mechanism, results are shown in table 5.

Table 5. "3-Joint" mechanism linear actuator peak values for force and velocity

Gait	Peak force generated by actuator, *N*	Actuator peak velocity, *m/s*
Walk	*1520*	*0,110*
Trot	*855*	*0,012*
Canter	*1080*	*0,052*

The results are quite close to those achieved earlier. However, peak values in case of "3-Joint" mechanism a slightly lower. Again, walk gait tends to have the highest force and velocity peak values and, thus, the highest power consumption. So, this gait was examined

more closely. Force generated by linear actuator and its linear velocity for the walk gait are shown in figure 27.

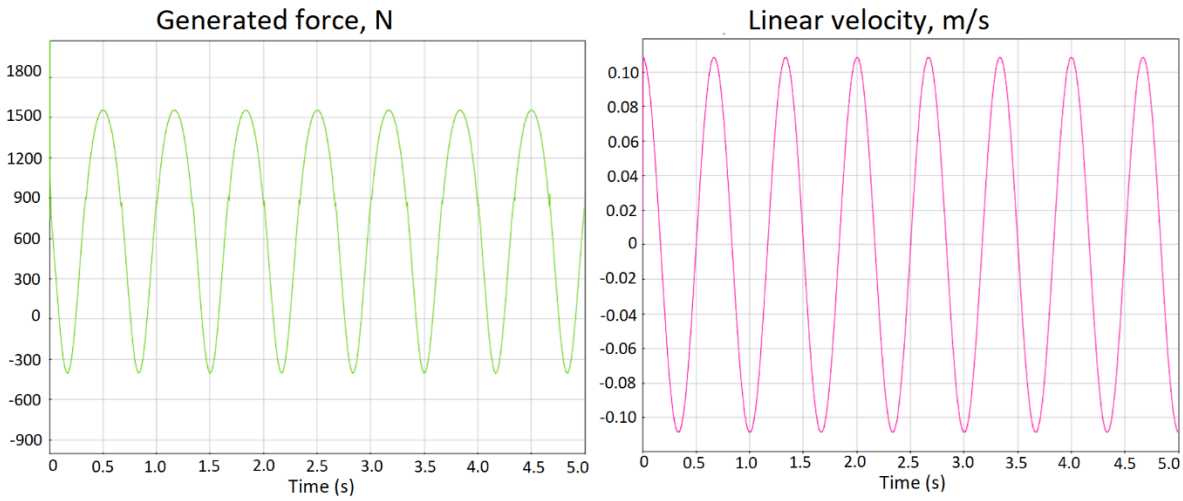

Figure 27. Force generated by linear actuator and its linear velocity for the walk gait in "3-Joint" mechanism.

These is also a phase shift between force and velocity in this case. Even though force required actuator force has not reduced significantly, the linear velocity is much lower than in "2-Joint" mechanism and that makes more compact and cost-effective actuator models available to use in this project. Thus, it makes sense to continue working with "3-Joint" mechanism and investigate linear actuator power consumption more closely, so it could be optimized later. Linear actuator power consumption plot is shown in figure 28.

Decrease of peak velocity allowed to decrease peak power consumption from *180 W* in "2-Joint" mechanism to only *120 W* in "3-Joint" mechanism. Part of this power was also used to overcome external forces of *100 N* average, that are caused by a rider pulling horse harness.

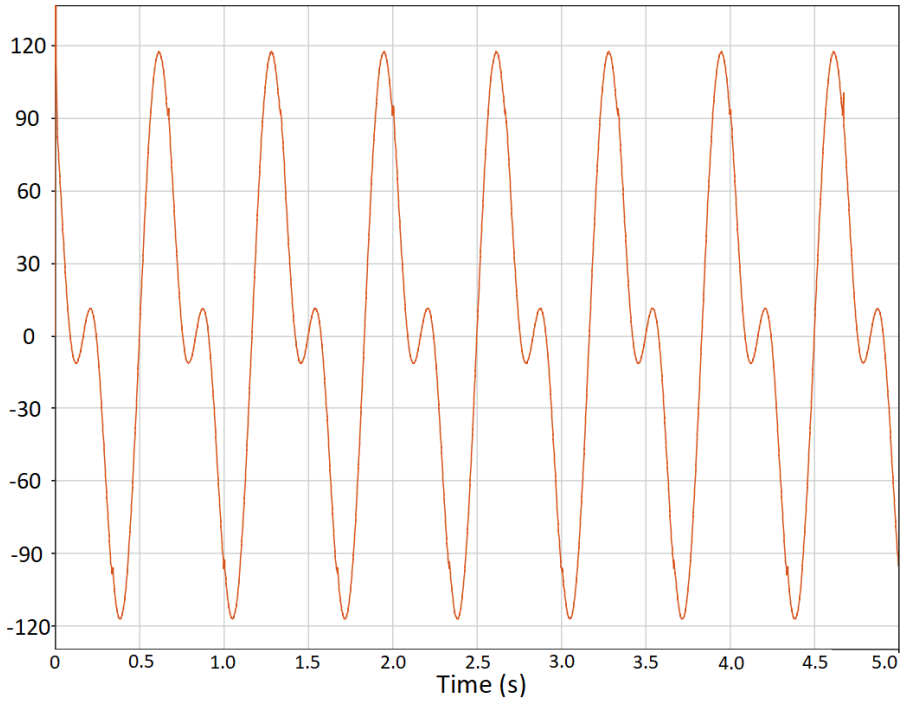

Figure 28. Linear actuator power consumption in "3-Joint" mechanism, *W*.

On the next step forces in joints were analyzed. Forces affecting the joints during simulation are shown in figure 29.

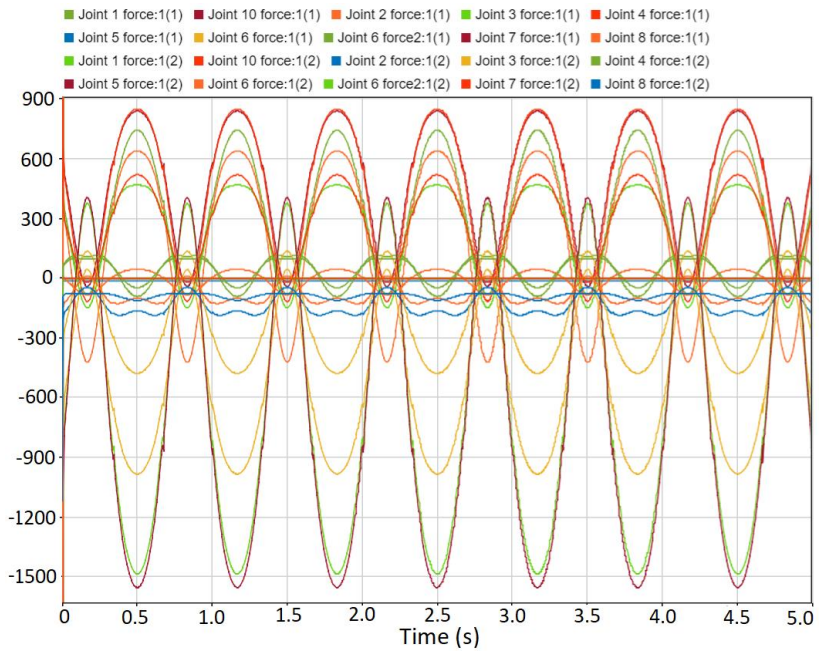

Figure 29. Forces (*N*) in joints during dynamic analysis of "3-Joint" mechanism.

The force distribution has not changed much from “2-Joint” mechanism. The joint “G” (figure 20) is still affected by the highest amount of radial forces. Their peak value is around *1500 N*. So again, extra attention should be paid to this joint whereas bearings in other joints are able to cope with loads easily.

Selection of the suitable kinematic scheme allowed to reduce power consumption by *30 %* and this is not the limit. It is possible to reduce this value even more. One of the possible solutions is use of counterweight. Implementation of this approach is due to mass concentration in simulator head area. Since head and neck mechanism represents a long cantilever beam with high amount of mass located on its edge, it causes high bending torques that significantly increase power consumption. Counterweight in this case can compensate gravity forces, but there are limitations of using it. Since the neck mechanism must be located inside of a limited volume which does not have any extra space for a counterweight, it must be located inside of horse simulator body. Yet it was possible to implement a counterweight, which is shown in figure 30 during simulation.

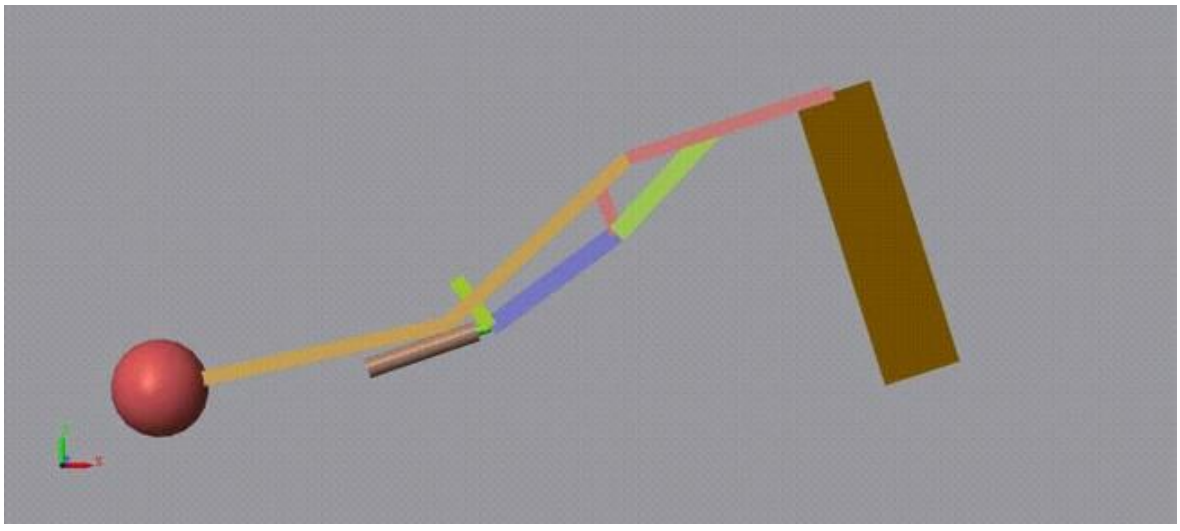

Figure 30. “3-Joint” mechanism with a counterweight during simulation.

Parameters of the counterweight: length and mass were defined manually based on several simulation results. An algorithmic optimization in this case would be unreasonable as it would consume too much time to implement without significant improvement of the results.

The final counterweight parameters are: mass – *5 kg*, length – *0,3 m*. Length cannot be increased because of geometrical limitations discussed earlier as it will start to interfere with horse simulator body. Further increase of any parameters will significantly increase moment of inertia and, thus, required force provided by actuator would also increase.

Now required actuator forces in mechanism with and without counterweight can be compared. The results of the simulation are shown in figure 31.

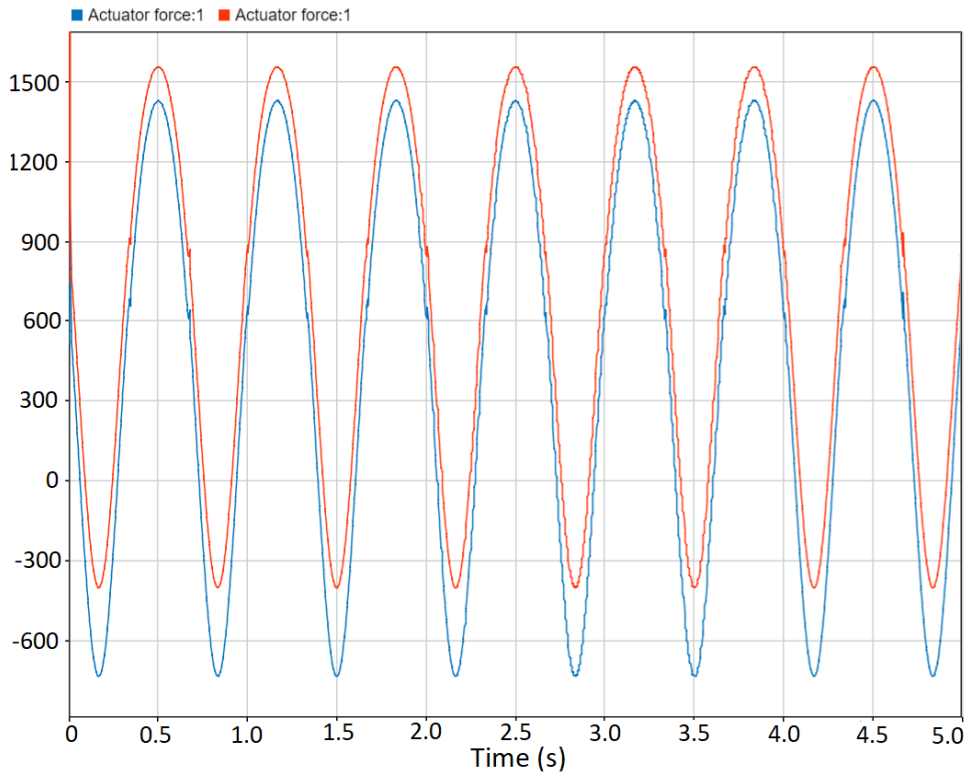

Figure 31. Required actuator forces in "3-Joint" mechanism with counterweight (blue) and without counterweight (red).

The counterweight reduces required peak pushing force by approximately *100 N*, however required pulling force is increased in this case by *300 N* due to increase of mechanism inertia. It seems that the difference is not that big as the counterweight reduced required force by only *6,7 %*, though a phase shift between velocity and force must be taken into account.

Therefore, the total effect of the counterweight may differ from the effect only on the required force value.

This is difficult to make conclusions without analyzing power consumption. Thus, it was done, and comparison of power consumed with and without the counterweight is shown in figure 32.

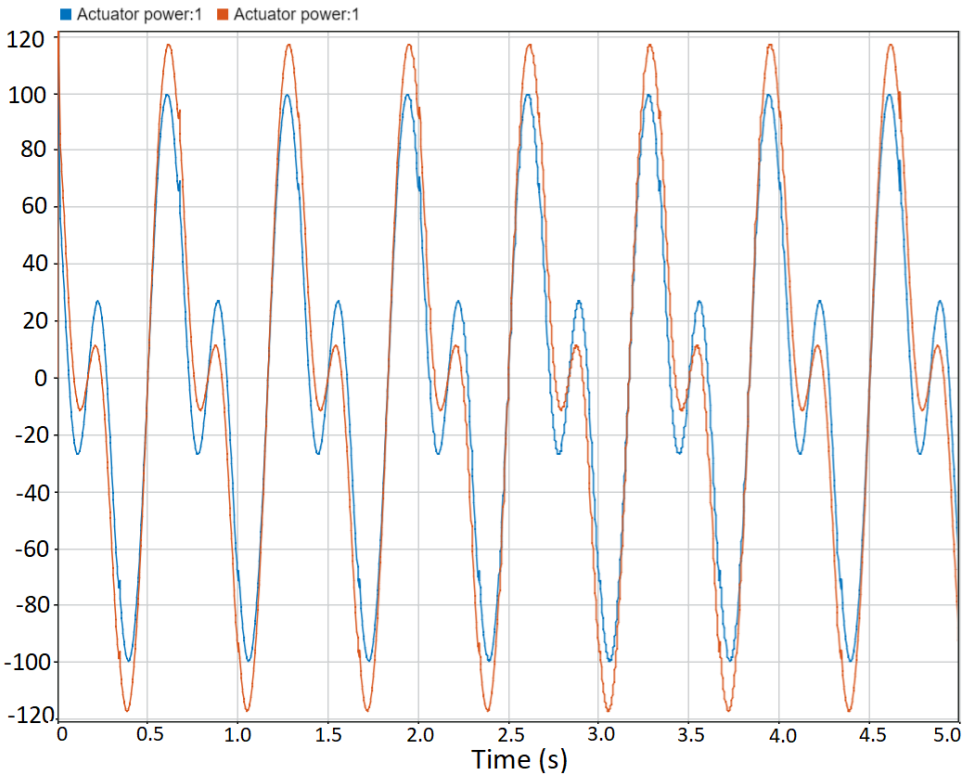

Figure 32. Power consumed by the linear actuator in "3-Joint" mechanism with counterweight (blue) and without counterweight (red).

It is clearly seen that the linear actuator without counterweight consumes almost *120 W* of power, whereas implementation of the counterweight reduces this value to *100 W*. It can be concluded that the counterweight contributes in *20 %* of peak consumed power reduction.

Achieved peak value of power consumption is much less than it was in the beginning and now it is possible to select a linear actuator that can fit inside of the simulator neck. It is also possible to replace the counterweight with a spring as in this way all inertia brough by the counterweight will be removed. And this option may increase energy efficiency of the mechanism even more.

After getting data about neck actuation, head part was considered. It was concluded that two revolution degrees of freedom is enough for horse simulator head to represent a realistic horse head motion. The head is actuated with use of two linear actuators, head kinematic scheme is shown in figure 33.

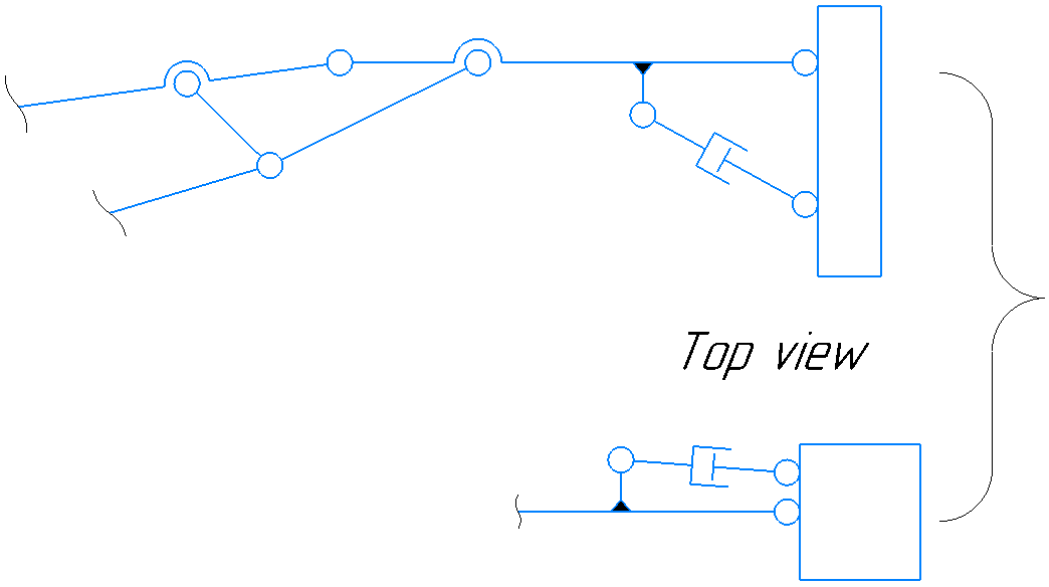

Figure 33. Kinematic scheme of horse simulator head.

Two linear actuators are located in the perpendicular plane. The actuator shown on the top view is responsible for motion in the horizontal plane and the other actuator is responsible for motion in the vertical plane.

Simscape model shown in figure 25 already contains solid block representing horse head and a revolution joint via which actuation is held. Actuation via revolute joint in simulation was modeled because on the stage of kinematic analysis it was not clear the exact positions where linear actuator would be attached. And even though the revolution joint cannot provide data about necessary actuation forces, information about total consumed power could still be obtained. Thus, selection of vertical head actuator was based on peak consumed power. Actuator responsible for horizontal motion is selected based on static forces caused by a rider pulling a harness. Since calculations for the horizontal actuator can easily be made manually, the actuator was not included in the model in sake of simplicity and computational time reduction.

The data regarding head actuator power consumption was already obtained from the previous simulation and the results are shown in figure 34.

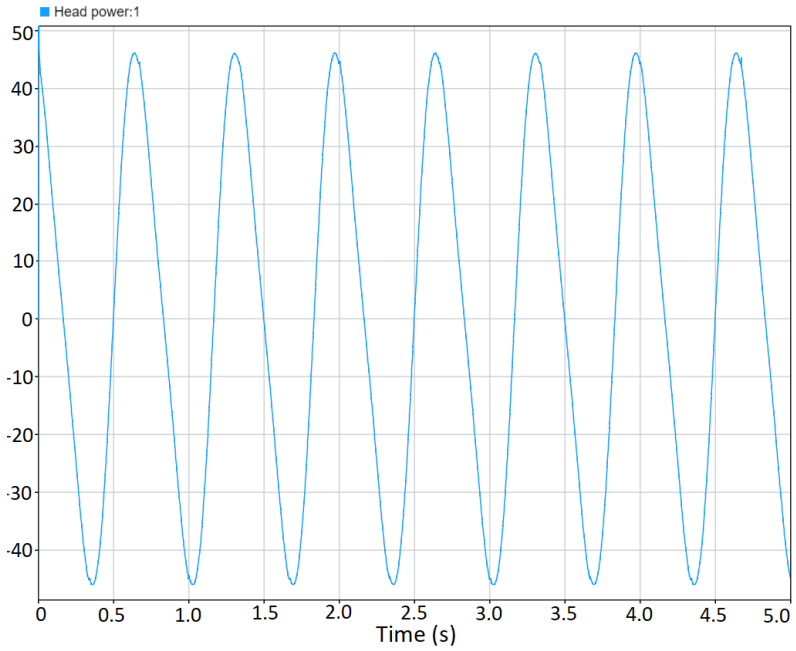

Figure 34. Head vertical actuator power consumption, *W*.

Head actuator power consumption is significantly smaller that then neck actuator consumption. According to simulation output peak power consumption is only *45 W*, nonetheless it is possible to reduce consumed power with use of springs.

The model that is shown up to this point is only the first iteration in development process. After achieving this data, the first CAD model was made. This first model helped to define dynamic parameters of the mechanism (such as mass and joint positions) more accurately. Due to geometrical limitations of a physical parts, lengths of some links were changed in the "3-Joint" mechanism, the new values are shown in table 6.

Table 6. Beams' new lengths in "3-Joint" mechanism

AB	*60 mm*
GJ	*260 mm*
HJ	*40 mm*
HF	*67 mm*
BF	*160 mm*
FL	*162 mm*
JL	*90 mm*
JM	*220 mm*

The lengths were changed in way that would not affect end effectors' outputs. So, the mechanism remains output that is shown in figure 20.

First CAD modeling has shown that there is no suitable linear actuator in the market that could fulfill the desired parameters for the head mechanism. Even after dynamics optimization neck mechanism requires too much power and force, so an actuator capable of providing the required force is too big and does not fit inside of the mechanism.

The solution of this problem is replacing linear actuator with a brushless DC motor with a gearbox and toothed belt transmission. This will allow to place the DC motor in the horse body and transmit rotation via toothed belt to the crankshaft "AB".

Another important decision that was made is replacing counterweight with springs. Due to requirements of mass reduction and low efficiency of the counterweight due to extra inertia, springs seems to be more effective solution.

Complete kinematic structure of the modified “3-Joint” mechanism is shown in figure 35.

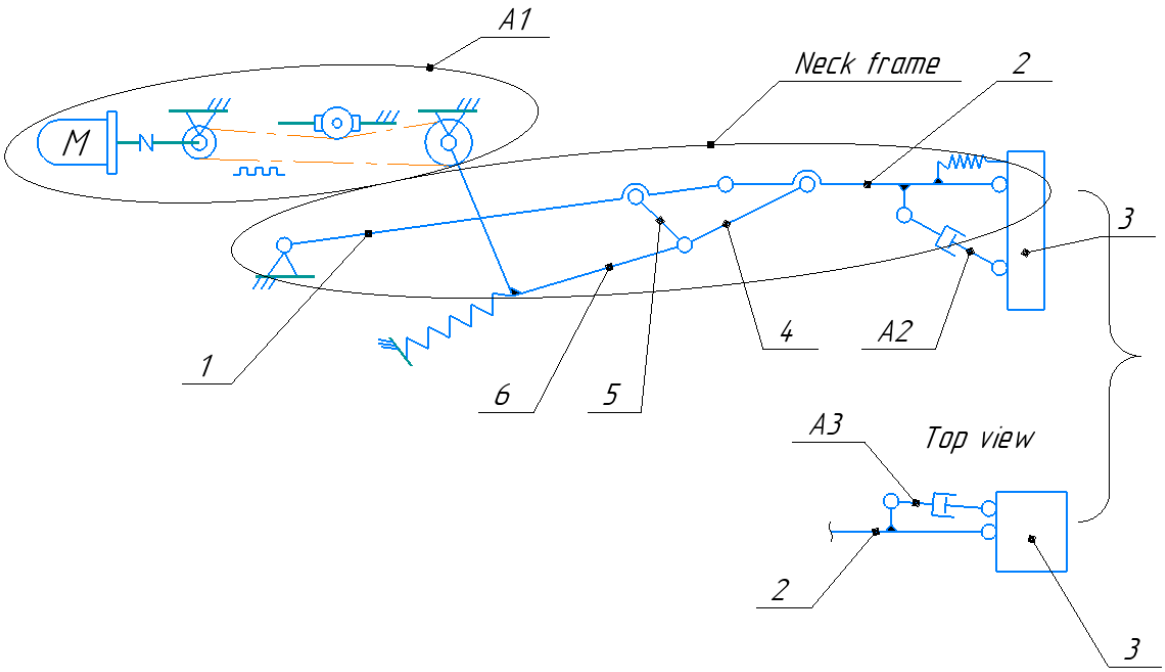

Figure 35. Kinematic structure of the modified “3-Joint” mechanism.

Now the structure of the mechanism is finalized and can be discussed. Main components of the mechanism are neck frame and head frame (3) shown on the Figure 35 and three actuators A1, A2 and A3. Neck frame is attached to an external frame (horse body) via a revolute joint. Neck frame consists of two main parts: crankshaft (1) and connection rod (2). Complex motion in the vertical plane of these two parts imitates motion of a horse neck. This complex motion is provided by actuator A1 and a drivetrain which contain crankshaft (6) and connection rods (4) and (5). Crankshaft (6) is also connected to an external frame; all elements of the drivetrain are connected via revolution joints. Actuator A1 consists of electric motor and a toothed belt transmission which provide revolute motion of the crankshaft (6). Linear actuator can also be used as the actuator A1.

Head frame (3) is connected to the neck frame via a spherical joint or a combination of revolute joints. Additionally, two linear actuators A2 and A3 connect the neck frame and the head frame. Actuator A2 provides head frame motion in the vertical plane, and actuator A3 provides head frame motion in the horizontal plane.

All actuators have integrated encoders. To provide required trajectories actuators are controlled by PLC with use of motor drivers and a feedback from the encoders.

Springs that connect crankshaft (3) to an external frame and head frame to the connection rod (2) can be used to reduce gravitational load on the actuators A1 and A2.

To select proper DC motor, gearbox and linear actuators more accurate results for torques and forces in the joints are needed. Due to this a new Simscape model was created. The model is shown in figure 36.

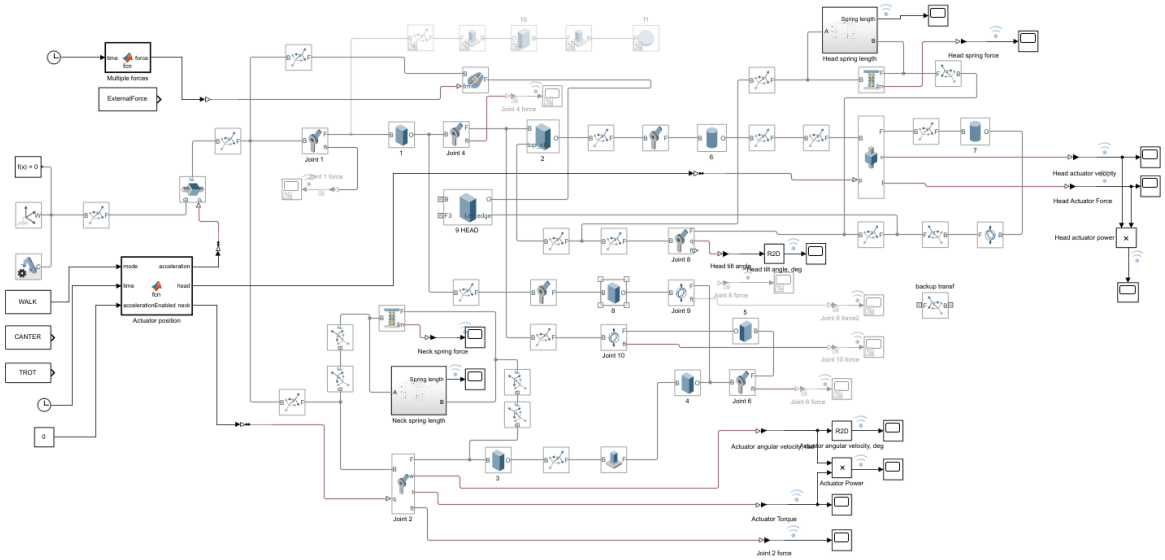

Figure 36. Simscape model of the modified “3-Joint” mechanism.

Some elements from the previous model are used in the new one, such as block for position control, beams’ bodies (lengths were changed) and some of the joints. Yet, a few joints were modified: a revolute joint that connected head and neck was replaced with linear actuator. This became possible after development of the first CAD model that gave an idea of the mechanism’s geometrical parameters. Additionally, this model takes into account springs, variable external pulling force and body vertical accelerations. The model during simulation process is shown in figure 37.

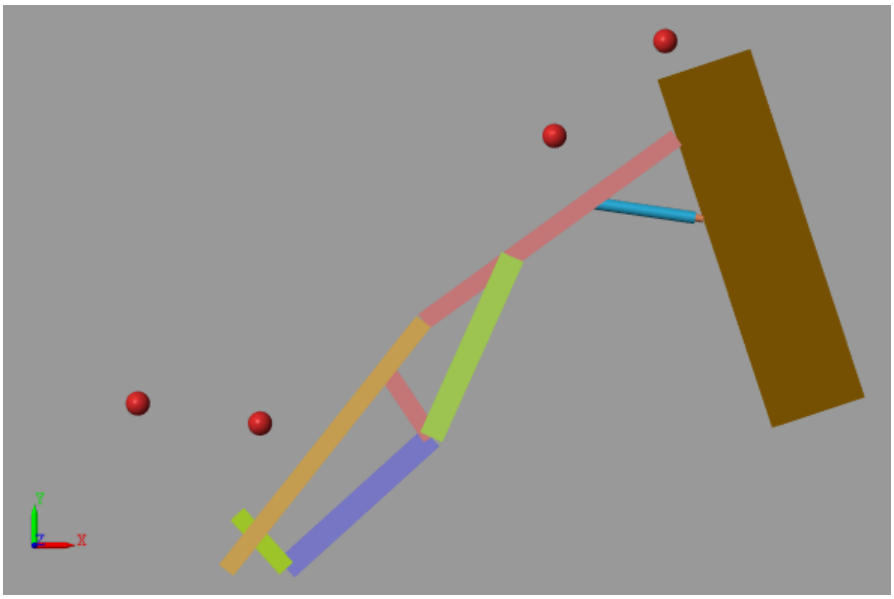

Figure 37. Modified Simscape model during simulation process.

Main beams of the mechanism are transferred to the new model, yet a linear actuator that was previously in the left bottom corner was replaced and a new head actuator was added. Another new feature that the model has is springs that indicated with the red dots. Two dots in the left bottom corner connect horse simulator body the orange beam in the figure. The Simscape mode does not represent the whole complex geometric of the head and neck mechanism, but the spring is still rigidly fixed. Another spring indicated with dots in the upper left corner connect pink neck beam and the head.

One thing that was changed in the model does not relate to physical bodies. For more thorough research the pulling force is now changing with time. The pulling force represents a rider who is pulling horse harness, at the beginning of the simulation this value equals to *0 N* and then it switches to *100 N.*

Even though the rider is capable of puling with greater force, it is not possible to pull harder for a long time and thus higher values will not affect on average power consumption. The force is provided by “Multiple forces” block that switches force value on the fifth second of the simulation. One of the goals in this case is to select optimal springs parameters that would minimize power consumption for both force modes.

As like as in the previous simulation, the walk gait turned out to be the most loaded gait and that is why all simulation results are shown for the walk gait. Nonetheless, the analysis was carried out for all three gaits.

The springs are discussed later and for now the results of the simulation that are shown in figures 38 and 39 can be considered.

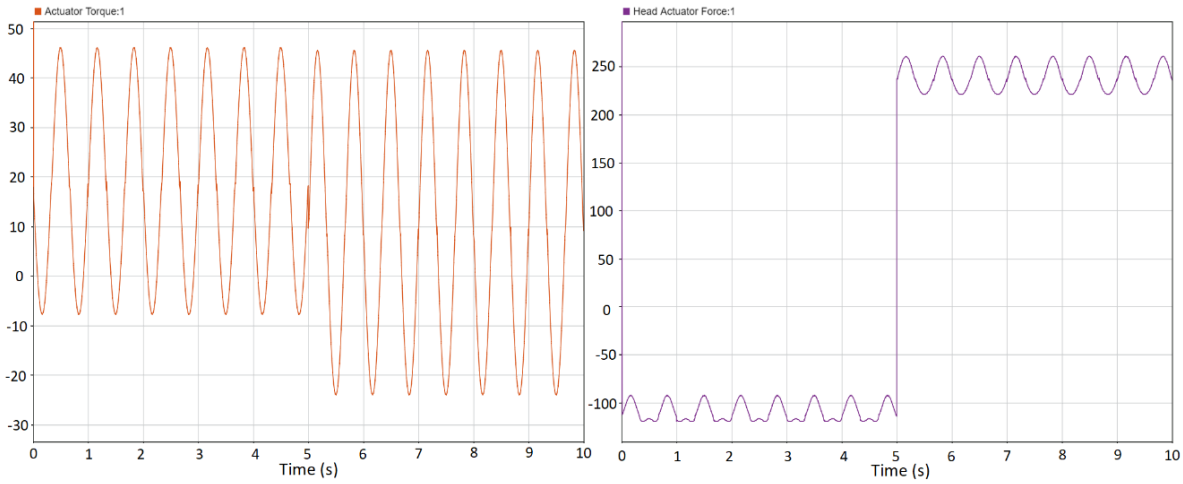

Figure 38. Neck actuator torque, *N*m* on the left and head actuator force, *N* on the right.

For the neck actuator increase of the pulling force requires additional torque when the head tilts down, however that does not affect the peak torque and thus does not increase peak power consumption.

The force in head actuator flips when the extra pulling force is added. This additional force switch actuator mode from working against extension to working against contraction in other words the actuator applies extra force needed to rise up the head. Peck force value in head actuator doubles with applying of the pulling force and thus doubles peak power consumption.

Now the power consumption of the actuators can be analyzed, simulation results are shown in figure 39.

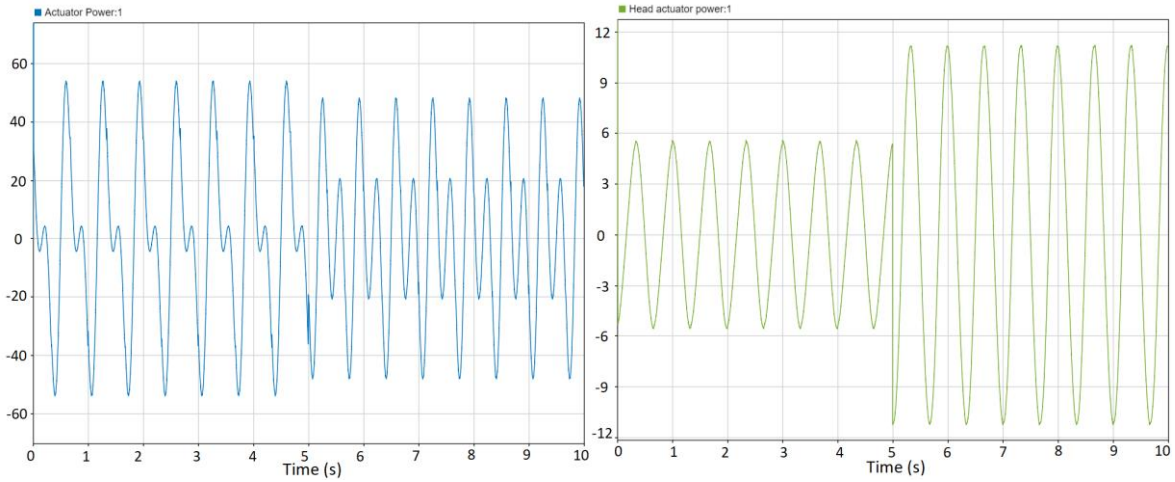

Figure 39. Neck actuator power consumption, *W* on the left and head actuator power consumption, *W* on the right.

Since the velocities of actuators do not change with pulling force applied, forces and power consumption plots have similar patterns. For the neck actuators was shown that its peak torque does not change and thus the power consumption does not increase. This is a good result as spring implementation provides almost constant peak power consumption for the head mechanism.

The results for the head mechanism are not as good as for the neck and the peak power consumption increases from *6 Watts* to almost *12 Watts* when the pulling force is applied. Nonetheless, these values are not high, and the head actuator satisfies power and force requirements.

Spring parameters were selected manually based on available coil springs parameters and geometrical limitations taken into account. Neck spring has natural length of *0.0897 m* and stiffness of *7350 N/m*. Since quite high stiffness is required the equal head spring was combined from three separate springs that are connected in parallel. The same approach was used for implementation of the head spring. It has following parameters: natural length of *0.1 m*, stiffness of *5820 N/m*. The head spring is also made as a parallel combination of two springs.

The forces acting in springs are shown in figure 40.

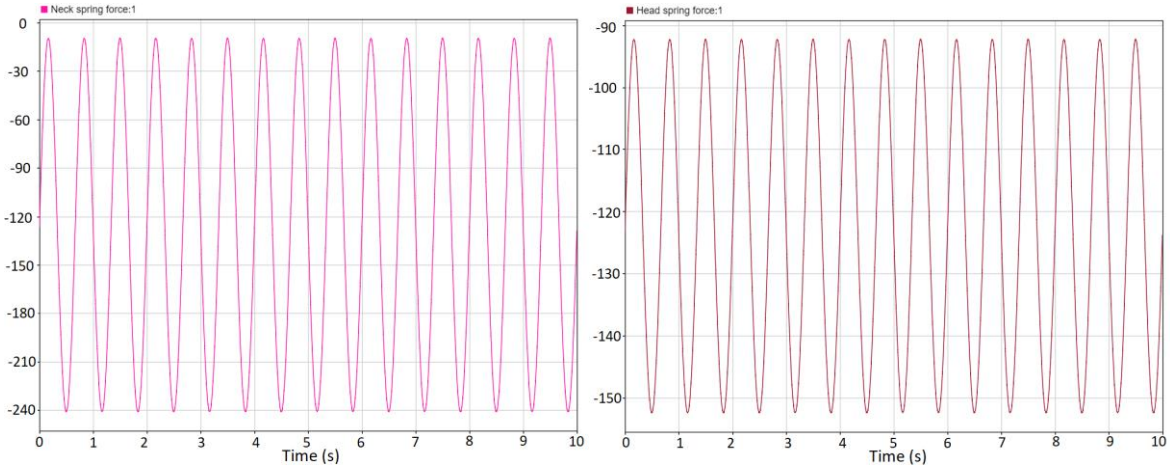

Figure 40. Forces in the neck spring, *N* on the left and in the head spring, *N* on the right.

Both springs are pretensioned and thus forces during motion does not reach. Negative force values indicate that springs are always extended. For the neck spring its length is varies from *92 mm* to *123 mm* and for the head spring from *116 mm* to *127 mm*. Peak stretching forces are quite big, for the neck spring it is *240 N* and for the head spring *150 N*. The reason why such small spring can withstand these values was partially explained previously: for both parts combined springs are used and the overall forces distribute equally between springs. This means that force that affects single spring of the head mechanism is three times lower than is shown in the figure and for the neck spring this value is two times lower.

The last important feature that makes this modified Simscape model more accurate is horse simulator body oscillations taken into account. The simulator is capable of providing vertical and horizontal accelerations with amplitude up to *3g*. The horizontal acceleration does not significantly affect the head and neck mechanism dynamics and thus the vertical acceleration will only be considered.

To implement a vertical acceleration a prismatic joint was added to the model. The joint connects the base frame and all the revolution joints that previously were fixed. An external signal is provided to the prismatic joints that controls its position, resulting forces are computed automatically. The position signal is generated in the “Actuator position” block that also generates signal for all the other actuators depending on selected gait type. The amplitude of the acceleration may vary from zero to three *gees*, according to the horse body mechanism specification. Frequency of the acceleration matches to the frequencies of neck

and head as in real life horse head and neck motion is a reaction for horse body vertical acceleration.

The analysis was carried out for all the gaits: walk, trot and canter and the same as the previous time the walk gait is the most energy consuming for horse head and neck motion. So, it will be analyzed carefully below.

The simulation was carried out for acceleration amplitudes from zero to three *gees* with a step of half *g*. The results of the simulation for *1g* and for *3g* accelerations are shown in figures 41 – 44.

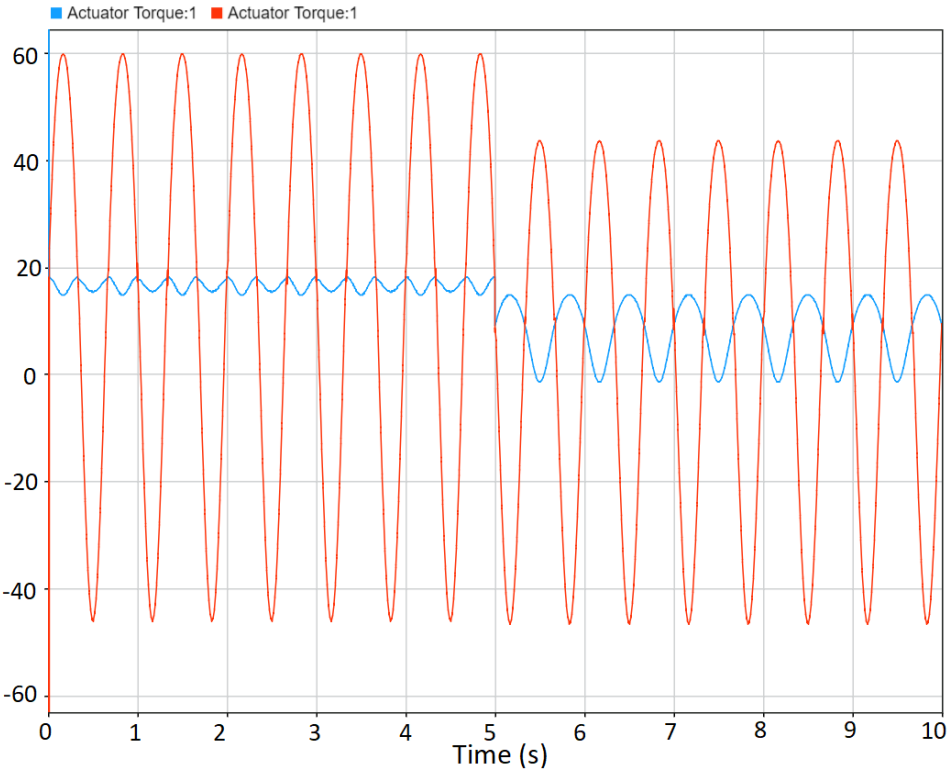

Figure 41. Torque in horse neck actuator, *N*m*, for *1g* accelerations (blue line) and for *3g* accelerations (red line).

As like as in the previous modeling with no accelerations, an extra pulling force is added on the fifth second of the simulation what causes torque amplitude to change.

It can clear be seen that motion under *1g* acceleration requires three times less torque from the actuator. In fact, work under *1g* acceleration requires two and a half times less torque than without acceleration at all. This is consistent with data acquired from living horse's analysis what confirms the correctness of the Simscape model.

Now a power consumption of the neck actuator can be considered.

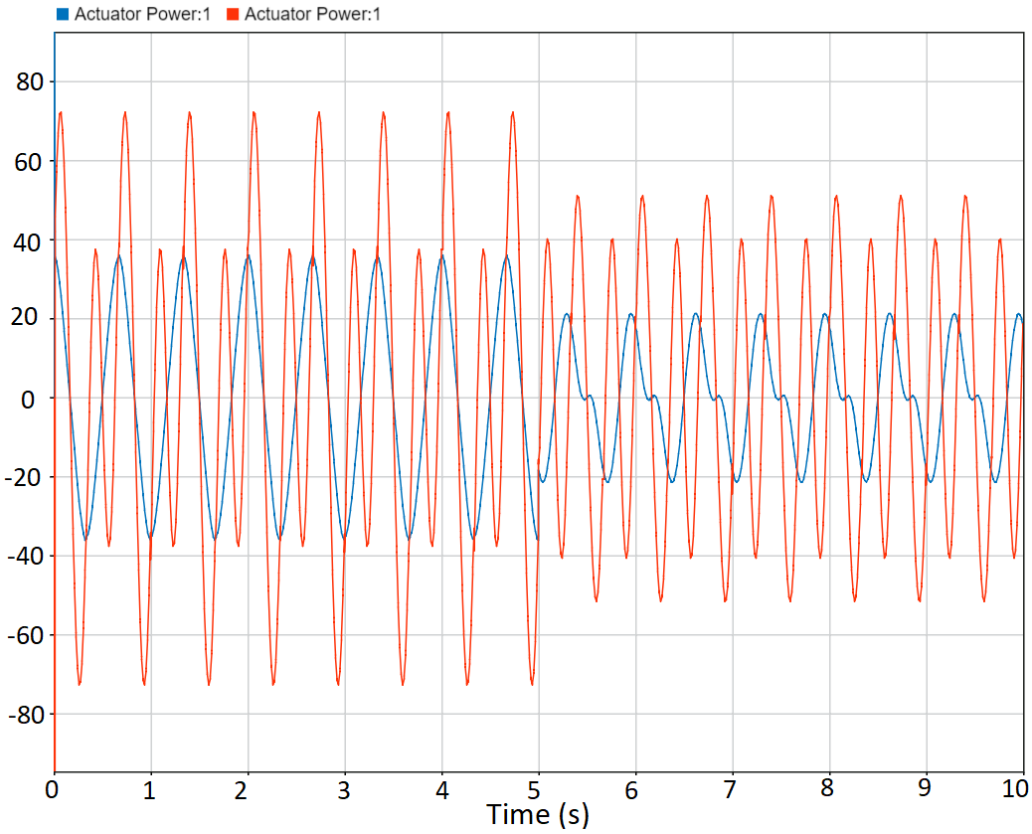

Figure 42. Power consumption in horse neck actuator, *W*, for *1g* accelerations (blue line) and for *3g* accelerations (red line).

The peak power consumed by the actuator under *1g* is *15 W* less than the power consumed with no accelerations and almost two times less than under *3g* accelerations. Increase of pulling force in this case works in the opposite way and helps to significantly reduce power consumption.

Energy consumption during 3g accelerations reaches *70 W*, but even this still relatively low. Approximately the same consumption value was reached with use of counterweight and

under no loads and even at that point it was a good result that was physically possible to implement. However, in current case *70 W* is a peak value under an extra load what demonstrates decent optimization results.

The same analysis carried out for the head mechanism is shown in figures 43 and 44.

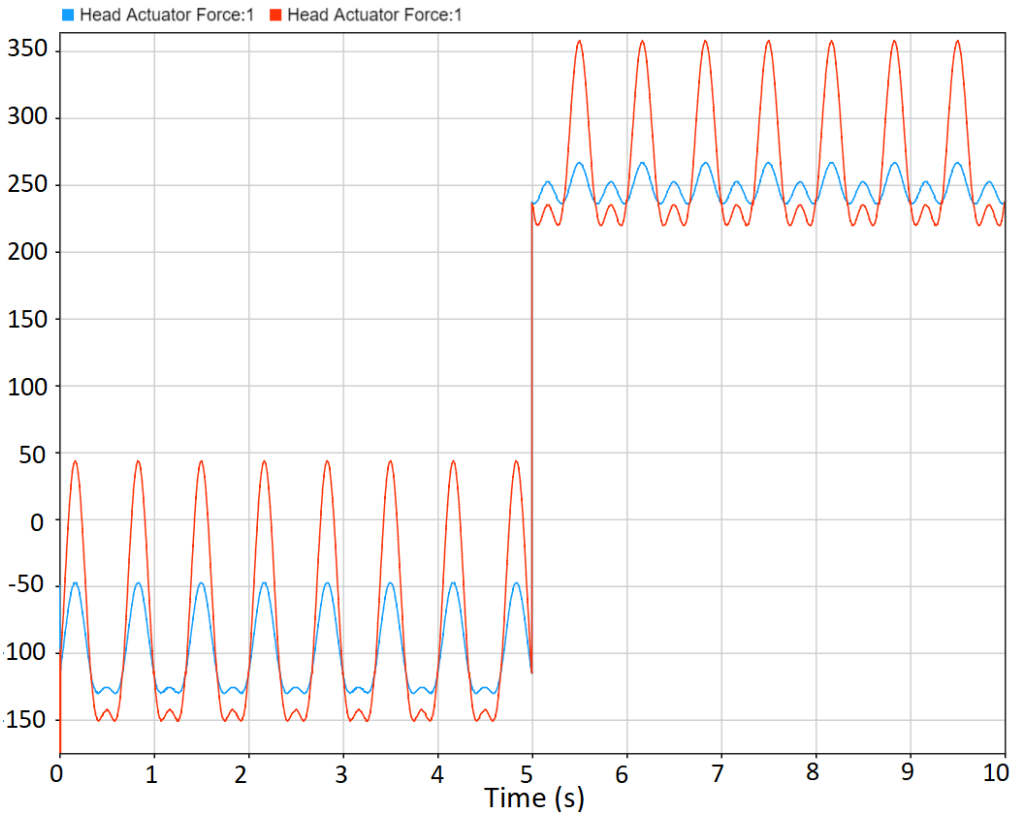

Figure 43. Force in horse head actuator, *N*, for *1g* accelerations (blue line) and for *3g* accelerations (red line).

The force distribution pattern remains the same in comparison to *0g* simulation. The force amplitude does not change much with change of external acceleration when the pulling force is equal to zero, whereas the force amplitude rises for *3g* acceleration. Compared to *0g* modeling, force amplitude in *3g* modeling is approximately *100 N* higher.

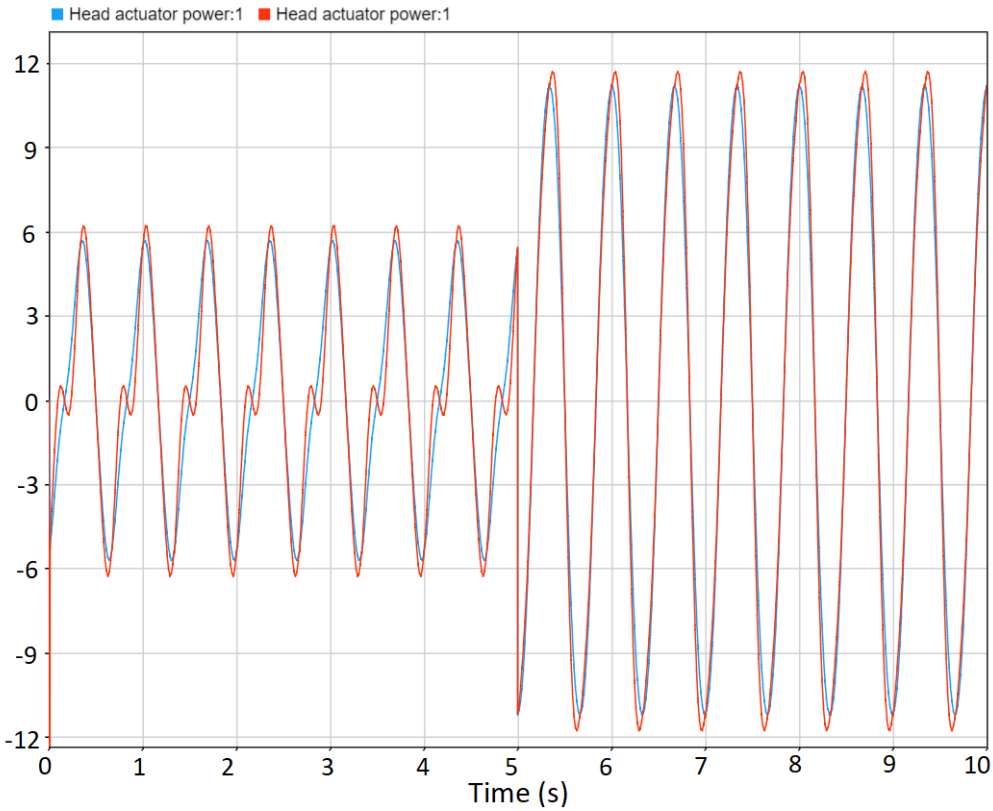

Figure 44. Power consumption in horse head actuator, *W*, for *1g* accelerations (blue line) and for *3g* accelerations (red line).

The power consumption of the head mechanism does not change much during different acceleration amplitudes of the horse body. Additionally, the peak power consumption for the mechanism remains the same for cases with no external accelerations and slightly below *12 W*.

Even though the forces applied to the mechanism reach *300 N*, linear velocity of the head actuator is very small and consequently the overall power consumption is also insignificant with peak value of only *12 W*. This small value is minorly affected by the changes of body acceleration in comparison to the neck mechanism.

The fact of different behavior under eternal accelerations can be explained in that the linear actuator of the head mechanism is almost parallel to the horizon. Thus, vertical forces crated by the acceleration do not affect the linear actuator and affect the head revolution joint instead. In the neck mechanism an opposite situation occurs as the neck actuator is fully affected by the vertical external forces.

The simulation has shown that the most loaded mode is a walk gait with horse body vertical acceleration amplitude of *3g*. This case causes actuators highest power consumption and external and internal forces have highest amplitudes. Thus, values acquired in this scenario will used during construction design process and during actuators and other equipment selection.

2.4 Construction design

The whole mechanism is based on a frame that is attached to a Gough–Stewart platform. Two possible options are considered for a frame material: it can be a welded frame from a low-carbon steel, or the other option is structural aluminum profile frame from which would be bolted. The advantage of first option, a steel frame, is its cost-effectiveness. However, this frame has a drawback of a heavy weight in comparison with aluminum frame. Yet, the aluminum frame has its own disadvantages of higher price and low rigidity due to screw connection of beams. Comparing both options, a conclusion of choosing a welded frame was made. Although, this type of frame is heavier, actuators which are used in the Gough–Stewart platform have enough load capacity to actuate whole body of a robotic horse including the head and neck mechanism.

Another major problem is safety. An equestrian's hands will always be close to a robotic horse neck as there is a necessity of holding a harness. Due to this fact the mechanism should be protected from getting finger or another body parts inside of it. One of possible solutions to this problem is an option used in a horse simulator made by Racewood Ltd.

An interesting part of this simulator is construction of horse neck. It has two revolute joints: one at the beginning of a neck and the second is in the interconnection of a head and a neck. Each of the joints have different types of protection from human limbs getting inside. Neck mechanism has a rubber cover around its joint which completely prevents equestrians from getting their finger or arms inside of it. However, head joint is less protected as it has a gap suitable for getting fingers inside. The safety in this case is provided by the fact that the neck joint is a revolution joint and the size of the gap does not change during operation of the

simulator, so even if a finger will get inside of the gap it will not be smashed by the mechanism.

In case of the designed mechanism the similar to Racewood neck protection can be used. A stretchy material can be attached around moving parts in order to protect an equestrian. This concept can be improved, and a stretchy material can cover all the neck. This will allow to the whole neck surface move and elongate during the motion like a natural skin making it look more realistically.

It was decided to use rubber as a material for skin imitation. The material is attached to hoops (7), (8) and (9) shown on the Figure 45. Hoop (7) is attached to an external frame, hoop (8) is attached to the head frame (3) and hoop (8) is connected to the end of crankshaft (1) via revolution joint and can freely rotate. The rubber can be used alone or in combination with another material that would imitate texture of a real skin. In the second case stretchy material is used as supportive underlay of another material and this material is wrapped around a stretchy material. One option for the outer material is artificial leather which will improve appearance of the neck.

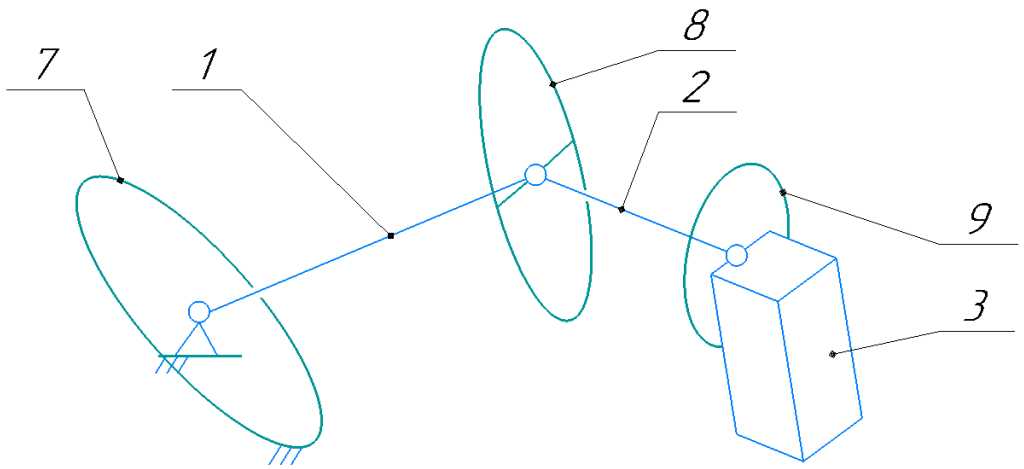

Figure 45. Scheme of hoops locations.

The material should be stretched around a frame that would shape a form of horse neck. This frame should provide enough space between moving parts and the “skin”, so that “skin”

would not be cut or damaged in any other way. A concept of this frame was designed and is shown in figure 46.

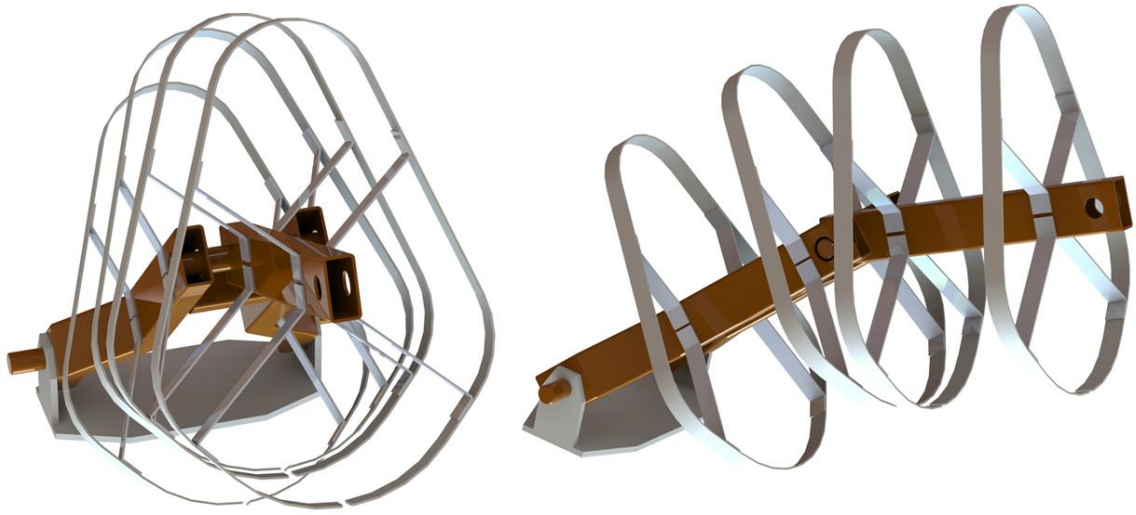

Figure 46. Frame forming shape of horse neck.

The frame consists of two cervical vertebrae beams. Metallic ribs are attached to these beams. Parts of the ribs are made from sheet low carbon steel and shaped with CNC laser cutting and bending, they are connected with rivets with each other and then they are bolted to the beams. The ribs have several sets of holes that are not shown in the figure. A stretchy material that imitates skin covers the ribs and then fixed to the with use of rivets. The figure represents only ribs locations and does not show the complete mechanical design.

Joints “A”, “E” and “G” (figure 20**)** can be designed with use of bearing housings. It is also possible to use milling to create housings to reduce mass and increase assembly speed, however this approach can noticeably increase cost which makes it questionable to use in the mechanism. The other joints (“B”, “F”, “H”) can be built with use of spherical plain bearings which are shown on the figure 47.

Figure 47. Spherical plain bearings.

Modern industry provides spherical plain bearings modification that does not require lubrication and additionally they are not vulnerable to misalignments what makes them the most suitable option for this mechanism.

Crankshafts and connection rods will be made from steel beams similarly to the frame. Interconnections between beams can be made from steel plates which are shaped with CNC laser. CNC machines in this case gives an opportunity to use topology optimization algorithms, which can slightly increase cost, but significantly reduce weight of certain parts. The upper connection rod is shown in figure 48.

Main parts of the upper crankshaft are bearings with housing, shaft, intermediate plates, and steel beam. The bearings are mounted on a base plate which will be shown later. M12 bolts are used to connect bearings and the base plate. The plate itself is rigidly attached to the simulator body frame, also with use of bolts.

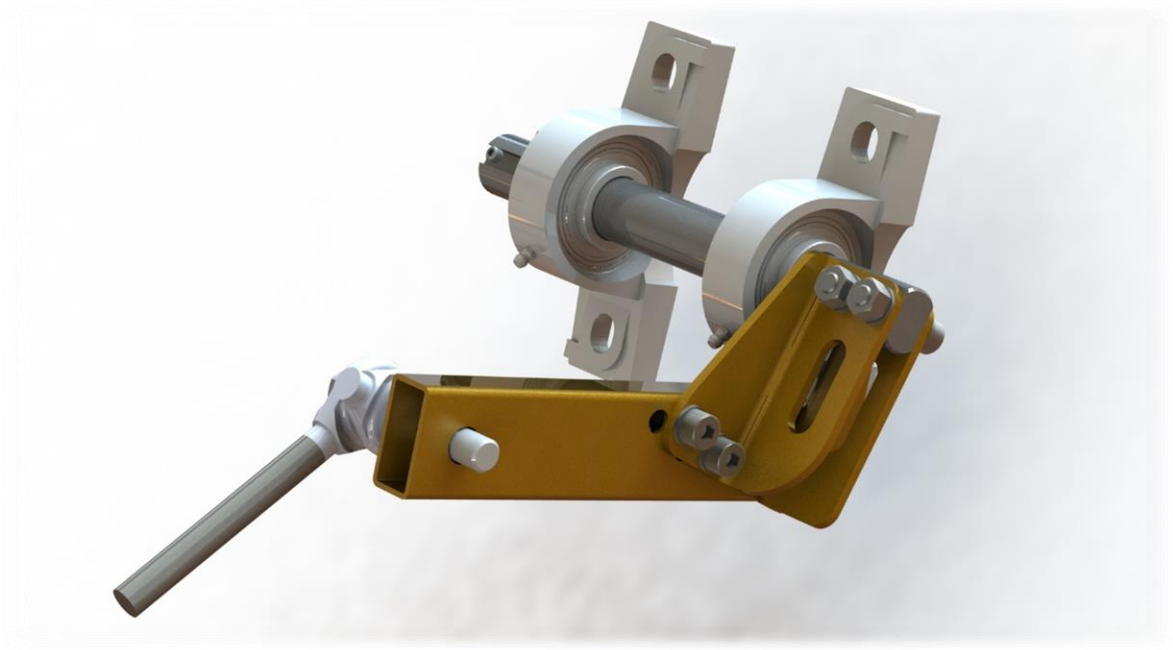

Figure 48. Upper crankshaft of “3-Joint” mechanism.

The shaft is fixed in-between the bearings and it has two milled surfaces to which intermediate plates are attached. The plates are bended from *4 mm* low carbon sheet steel and bolted to the shaft and to the steel beam. It was also possible to use welding instead of bolts in this case, however it would require more complex shaft shape and it would increase manufacturing cost. Almost at the end of the beam a hole is drilled for another shaft. This shaft is used to connect plain bearing shown earlier to the beam.

Another part that is attached to the base plate is lower crankshaft that is shown in figure **49.** Design is quite similar to the previous crankshaft, but in current case different type of housing bearings is used, and these bearings are connected to the base plate via extra angled plates from *2 mm* sheet steel.

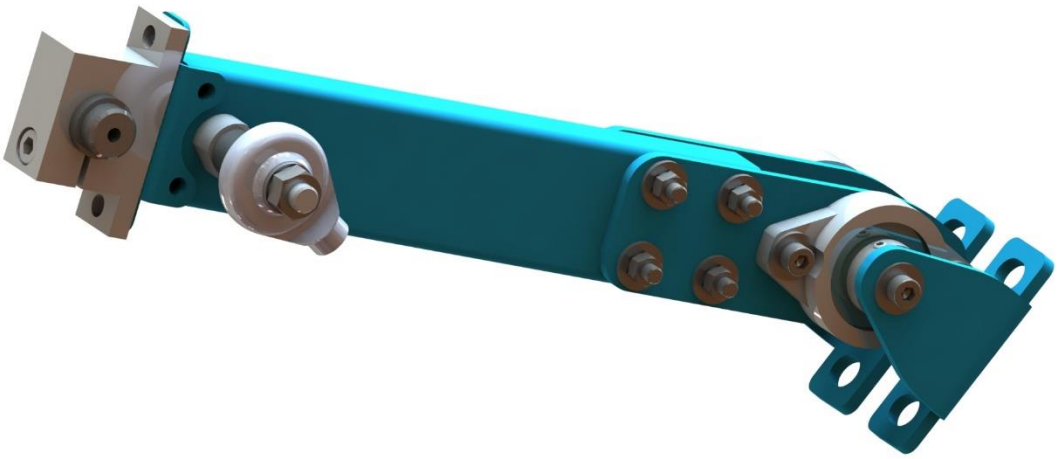

Figure 49. Lower crankshaft of "3-Joint" mechanism.

Because of the desire to minimize welding and optimize assembly cost all the parts are bolted. The beam in the middle is attached to the bearings via *4 mm* thick plates. On the other end of the beam a shaft housing is attached to it via a flange that is also made from sheet metal. The shaft housing will be used to fix a shaft which connects the lower crankshaft to the connection rod. Almost half of the used parts are mass produced and easily can be ordered from suppliers, since the approach of manufacturing as fewer custom parts as possible may reduce total cost and assembly time.

Each of the crankshafts are connected to the base plate and they are interconnected via rods with plain bearings. The subassembly is shown in figure 50. The orange plate on the drawing is the base plate. It is made from *4 mm* sheet metal and bended. The bended edges of the plate a welded together to increase part rigidity (the welding is not shown on the figure). Directly on the bends several slits are made. This is done to simplify a manufacturing process as it will be much easier to bend a part with weakened edges, nevertheless it does not affect on overall rigidity or strength.

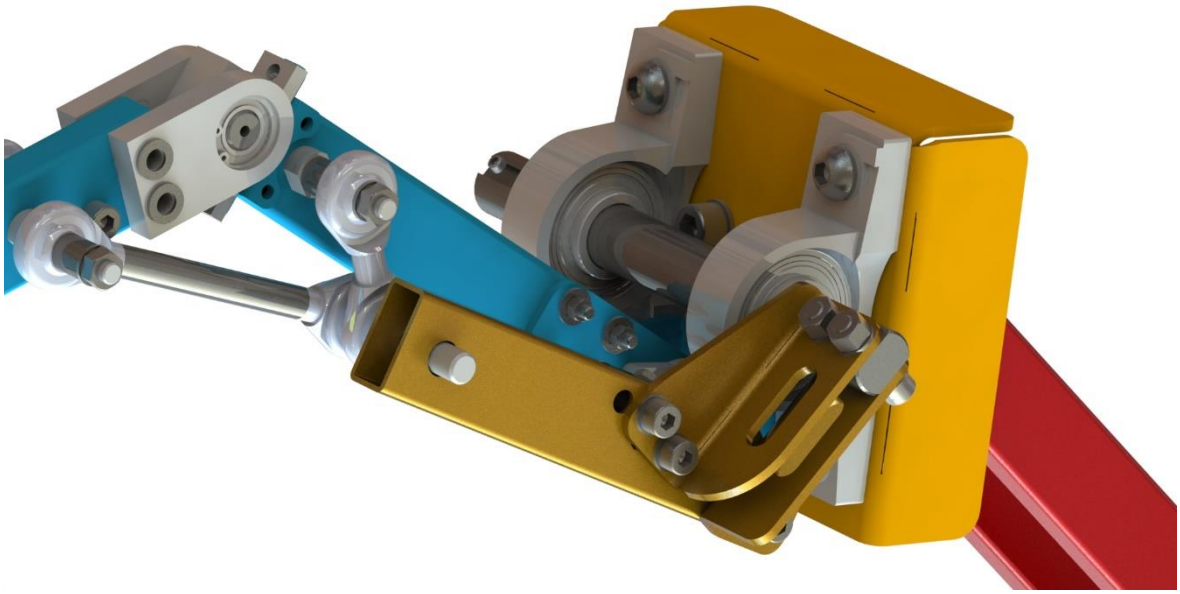

Figure 50. Subassembly of crankshafts on the base plate in “3-Joint” mechanism.

The whole mechanism is attached to the simulation body frame, that are red beams which can be seen in right bottom corner of the figure. The red beams are connected with use of welding. They form a flat rectangular frame that is easy to transport. Use of welding in this case allows to get rid of extra flanges and other parts, minimizing weight and assembly time.

Connection rod that connects crankshafts and horse head is also made from steel beam. It is connected to the upper crankshaft via a rod with plain bearings and to the upper crankshaft via bearings with housings. On the right and left sides of the connection rod linear actuators are located. These actuators provide motion to the red plate on figure 51. The red plate is a base to which the rest of the head will be attached. Two pairs of bearings with housings are located at the end of the connection rod to provide two revolution degrees of freedom to the head.

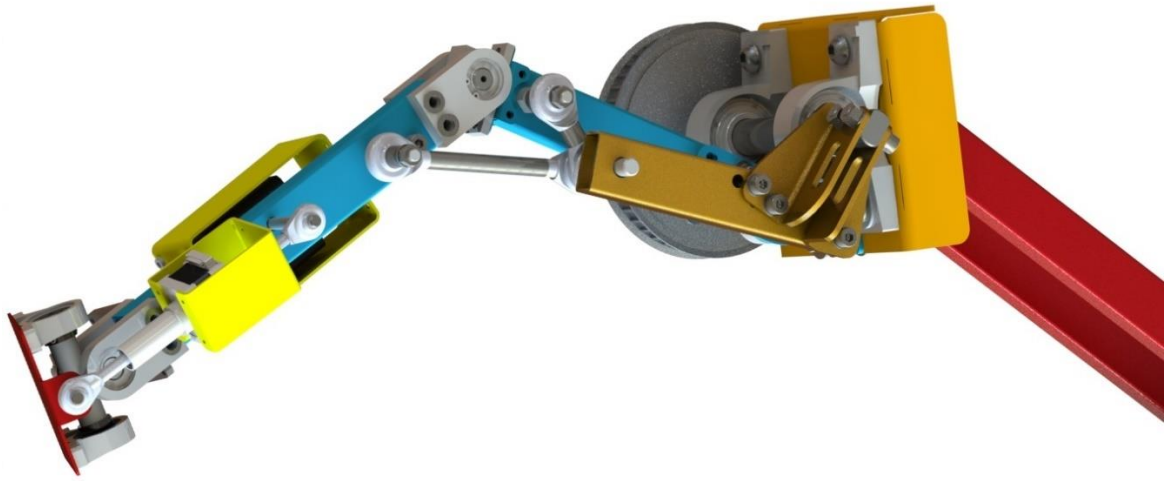

Figure 51. Initial mechanical design of the head and neck mechanism.

The last part of the mechanism is a counterweight which is used to reduce power consumption of the linear actuator. The “G-H” beam (figure 20) can be extended to attach the counterweight that can be made of steel plates with use of CNC laser cutting. A set of different counterweight plates can give an ability to adjust counterweight mass during experiments with a prototype.

However, this approach will require higher amount of custom manufactured parts and will increase total coast and mass of the mechanism. In the simulation section it was shown that the mechanism which uses springs instead of the counterweight has higher efficiency. Therefore, it was decided to replace a counterweight with springs that would provide the same peak force as counterweight does. This approach will reduce cost since spring are mass produced and they can be easily integrated into existing solution.

The figure above is simplified and shows not all the parts of the assembly. Other researchers involved in the project provided horse body CAD model and the mechanism was integrated with it to check how if it fits perfectly. The mechanism combined with horse body CAD model is shown in figure 52.

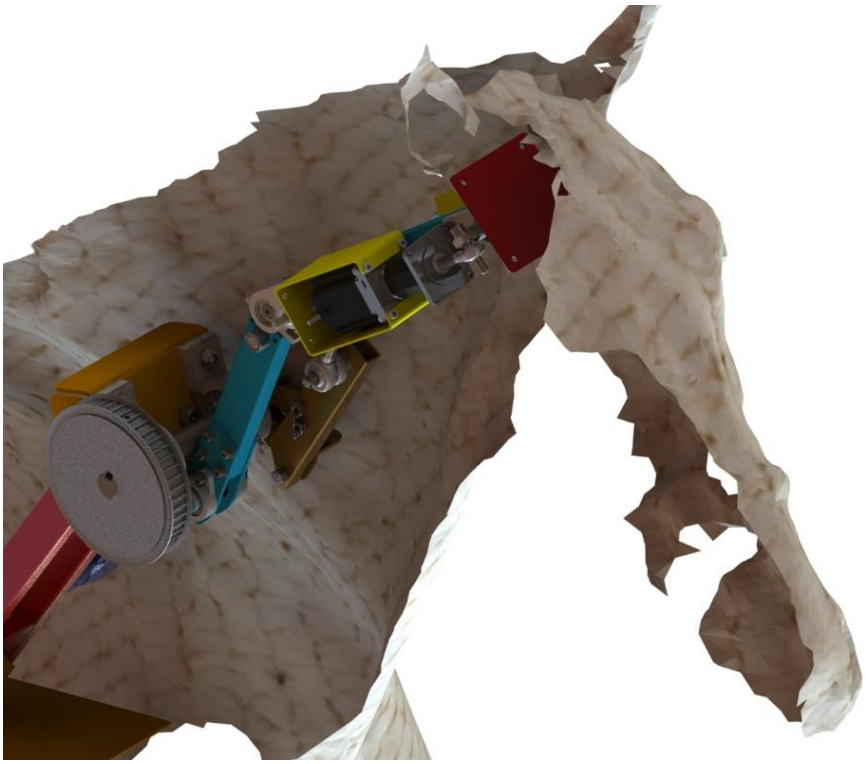

Figure 52. Horse head and neck mechanism combine with horse body CAD model.

The model shown on the figure above represents the first iteration of the CAD model. This model allowed to refine the data masses, dimensions, and other properties. That gave a better understating on how mechanical parts should be located. The data also was used to improve quality of the Simscape model and after analyzing of the results, an improved CAD model must be made.

The modifications were started from the neck drivetrain. A linear actuator was replaced with a brushless DC motor. There was not enough space in the neck and motor had to be moved inside of the horse simulator body. A toothed belt transmission is used to deliver torque from the motor to the crankshaft.

The Simscape modeling has shown that the motor should provide torque of at least *60 N*m* and the output power of the motor must be at least *80 W*. Small motors that can fit inside of the body cannot provide such high torque, so a gearbox was used. The gearbox was installed after the motor and before a toothed pulley.

After a market research the most suitable motor was found. That is PD4-EB59CD-E-65-1 – a brushless dc servo motor with integrated controller, NEMA 23 flange size and integrated single-turn absolute encoder. Its parameters are shown in table 7.

Table 7. PD4-EB59CD-E-65-1 DC motor parameters

Rated power	*220 W*
Rated speed	*3500 RPM*
Peak current	*18 A*
Operating voltage	*12 VDC – 48 VDC*
Rated torque	*0,6 N*m*
Interface	EtherCAT

The motor rated power is significantly higher that required. There are several reasons for that: the Simscape model does not take friction in the "3-Joint" mechanism into account, motor and gearbox has efficiencies less than *100%* and lastly, there must be a power margin in case of overloads.

Output torque of the motor of the motor is very low what required use of a gearbox. As the drivetrain also includes a toothed belt transmission it was decided to increase the torque in two steps: firs, the rotation transmits to a gearbox with a gear ratio of *1:40* and then the motion comes through the toothed belt transmission which has its own gear ration of *1:3*. The total gear ration in this case is *1:120* and, consequently, the maximum output torque that comes from the toothed belt transmission is *72 N*m*.

The gearbox reduces output angular velocity, so it must be checked if it still satisfies the requirements. The maximum required angular velocity is *120 degrees per second*. The motor rated speed is 3500 rpm, thus the output angular velocity equals $\frac{3500\ rpm}{120 \cdot 60s} \cdot 360° = 175\ \frac{degrees}{second}$ that totally satisfies the requirement.

The installed gearbox is a precision planetary gearbox GPLE60-2S-40 integrated with the motor. Gearbox parameters are shown in table 8.

Table 8. GPLE60-2S-40 precision planetary gearbox parameters

Reduction ration	*40*
Max. output torque	*64 N*m*
Admissible axial shaft load	*450 N*
Admissible radial shaft load	*340 N*
Service life	*30000*
Max. input speed	*13000 RPM*

The motor with the gearbox is mounted on a flange that is fixed to the horse simulator body frame. The torque from the gearbox transmits via coupling to a toothed pulley. The pulley is fixed on a shaft that is mounted on two bearings with housings. CAD model of this assembly is shown in figure 53.

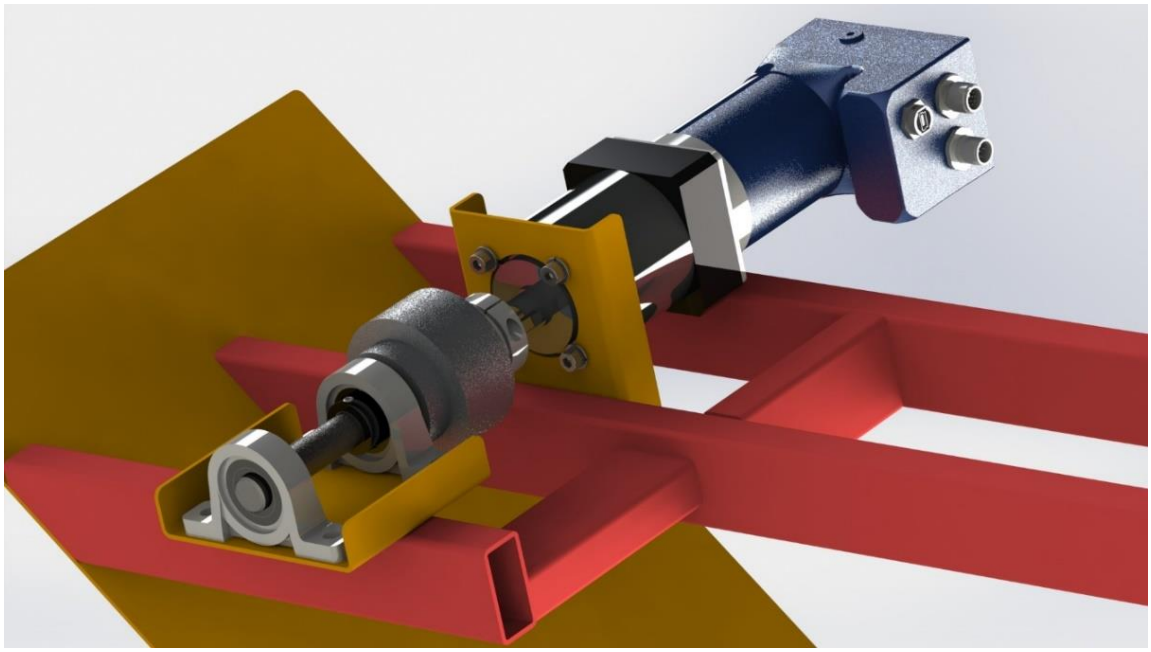

Figure 53. CAD model of the drivetrain.

The toothed pulley on the figure is simplified. The toothed belt transmission uses AT10 belt type and the corresponding pulleys. A set of idler pulleys is fixed to the horse body frame to provide necessary tension of the belt.

The construction that includes bearings is necessary to eliminate all radial forces from the gearbox shaft in order to increase its service life. The coupling is used in order to eliminate

all forces caused by misalignment what also increases service life of the gearbox and the bearings.

The new simulation results also required modification of the other parts of the mechanism. For the upper crankshaft set of springs was installed and the design of the crankshaft itself was improved. The new upper crankshaft is shown in figure 54.

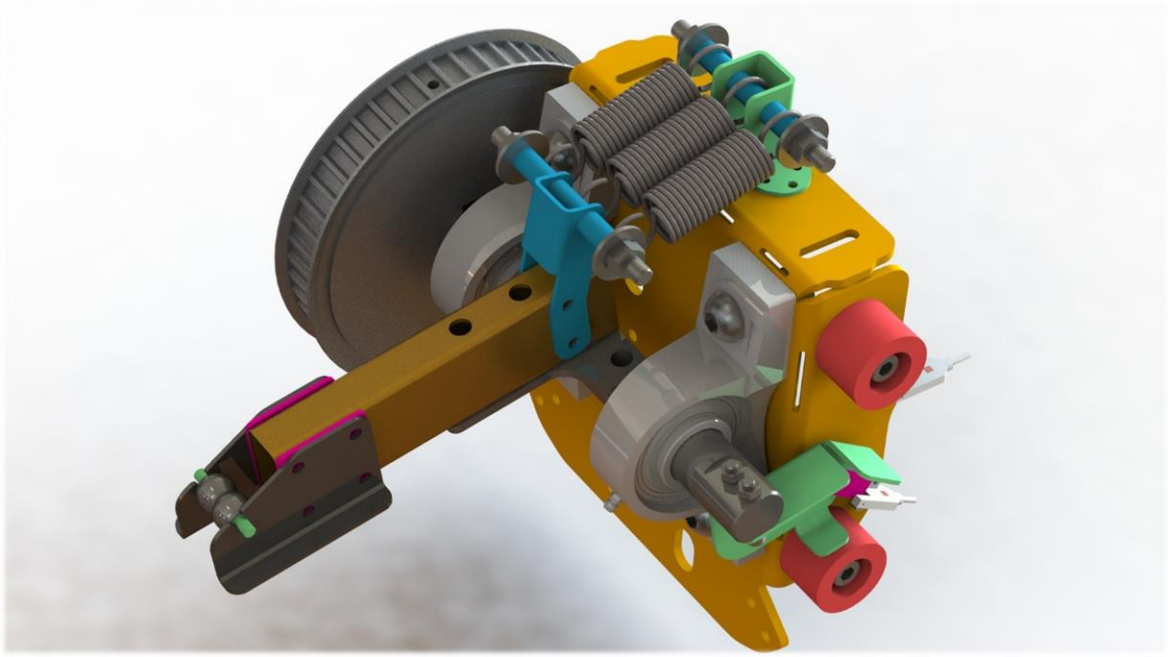

Figure 54. CAD model of the modified upper crankshaft.

The crankshaft previously was a combination of two beams that formed an angled construction. It was possible to simplify the design and implement the crankshaft with use of only one main beam. A blue hinge is fixed to this beam and another green hinge is attached to the orange base plate. These hinges are used to fix springs in-between them.

The beam is fixed on a shaft that is mounted on two bearings with housings. A pulley with 48 teeth is attached to the shaft. Use of a big diameter pulley is caused by implementation of an additional gear with toothed belt transmission.

Two red dampers are attached to the base plate on the right. A corresponding green lever is fixed on the shaft and thus motion of the shaft is limited by these two dampers and the lever. This is needed to prevent the upper crankshaft from rotating too high or too low if a program

error occurs or electricity supply fails. The green lever also has a flag that moves through an optical limiter switch. This sensor is used to calibrate the mechanism after it is turned on as the actuators use incremental encoders and they cannot provide accurate position data without calibration.

The lower crankshaft also was modified. The new CAD model of the lower crankshaft is shown in figure 55.

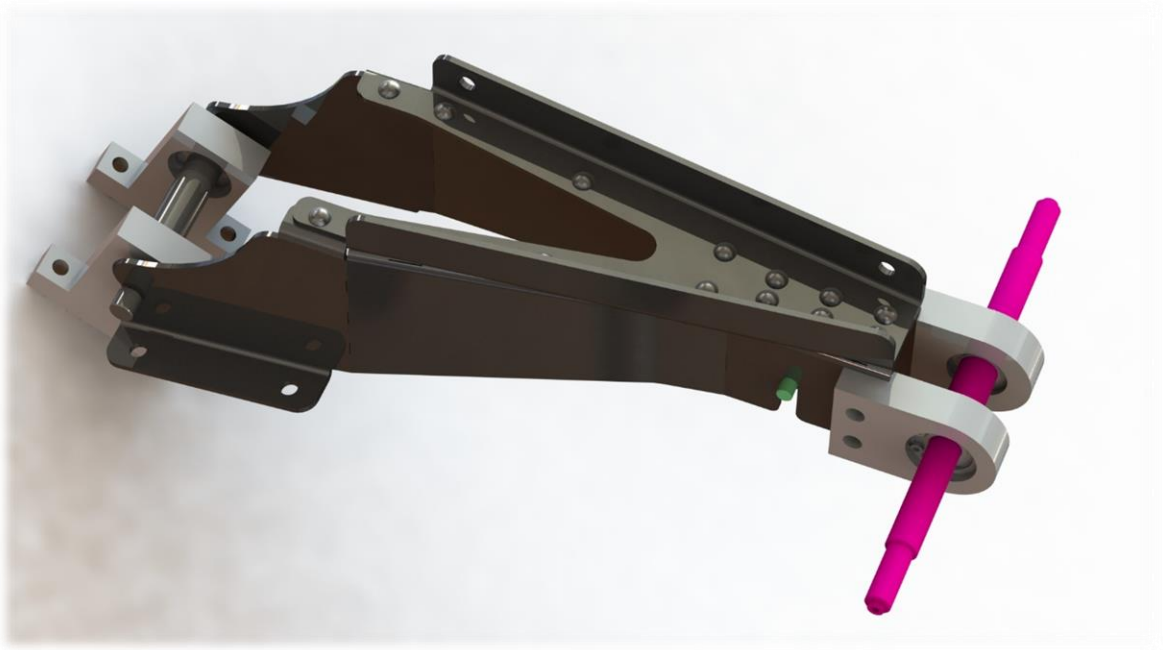

Figure 55. CAD model of the modified lower crankshaft.

Now the crankshaft is made from bended sheet metal with *2 mm* thickness. The plates are fixed with rivets to each other. The crankshaft has a long gap through which the lower crankshaft passes. This approach allowed to save space inside of the mechanism and improve integrity of the assembly. Consequence of this is higher material saving.
Pink shaft on the right is used for two purposes. First of all, a connection rod is attached two it and secondly an outer frame that is used in forming of the neck shape is also fixed on the pink shaft.

The connection rod cannot be considered without the head mechanism, both parts are shown in figure 56.

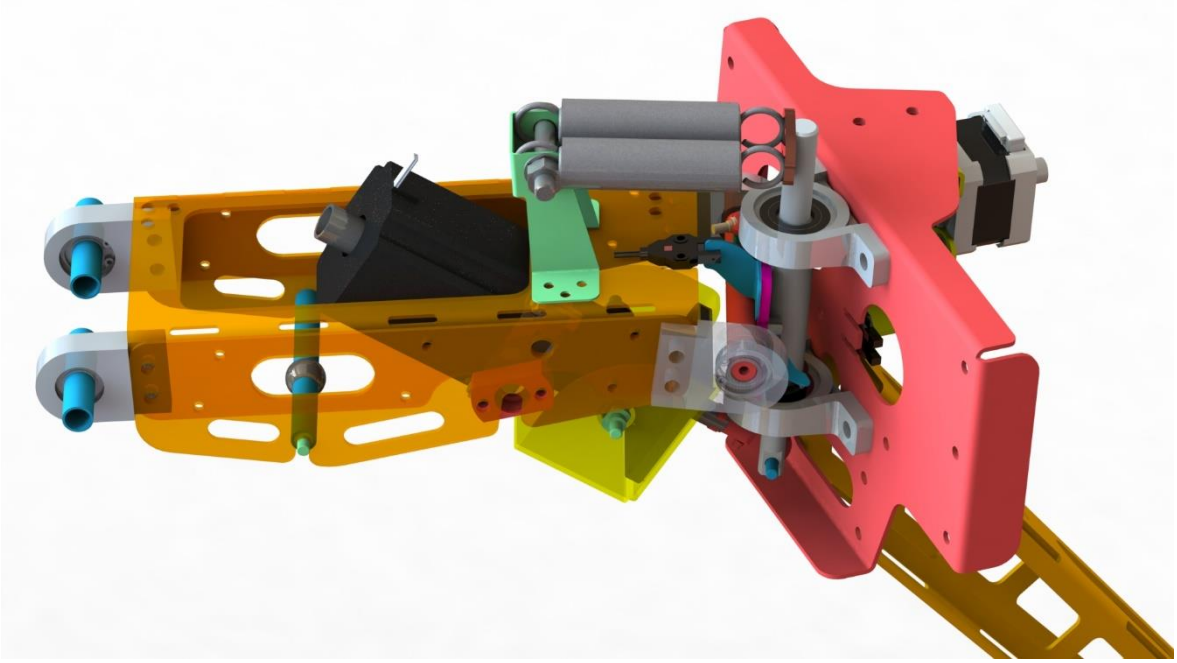

Figure 56. CAD model of the connection rod and the head mechanism.

The connection rod has bearings on the both ends. It is attached to the lower crankshaft on the left and to the head mechanism on the right via bearings. The rod has U-shape and consists mainly from bended sheet metal with *2 mm* thickness.

Inside of the connection rod the linear actuator is located. The actuator is responsible for head vertical motion. The actuator has a yellow flange that has two bearings with housings. These bearings are connected to the intermediate part of the connection rod. This design will allow the actuator to rotate freely in the vertical plane if it is not connected to the head mechanism. Yet, these parts are connected via a spherical plain bearing that is attached to the end of the actuator.

The actuator was selected based on the data from the simulation: its maximum power consumption must be at least *12 W* and provided axial force is at least *350 N*. A suitable option in this case is captive linear actuator L5918L3008-T10X2-A50. Its parameters are shown in table 9. The actuator has an incremental encoder for feedback.

Table 9. L5918L3008-T10X2-A50 captive linear actuator parameters

Max. axial force	*1000 N*
Stroke	*50 mm*
Speed	*80 mm/s*
Resolution	*0.01 mm/step*
Max. power output	*20 W*

The connection rod and the head mechanism have the third connection via springs. To mount the springs on the connection rod a green hinge from *1 mm* thickness sheet steel is used. On the other side these springs are fixed to the *4 mm* thickness plate of the head mechanism. An optical limiter switch is fixed on the connection rod for actuator encoder calibration. The head mechanism has a corresponding flag for the limiter switch that triggers the sensor when head reaches its lowest position.

The last part is the head mechanism itself that is considered separately. CAD model of the head mechanism is shown in figure 57.

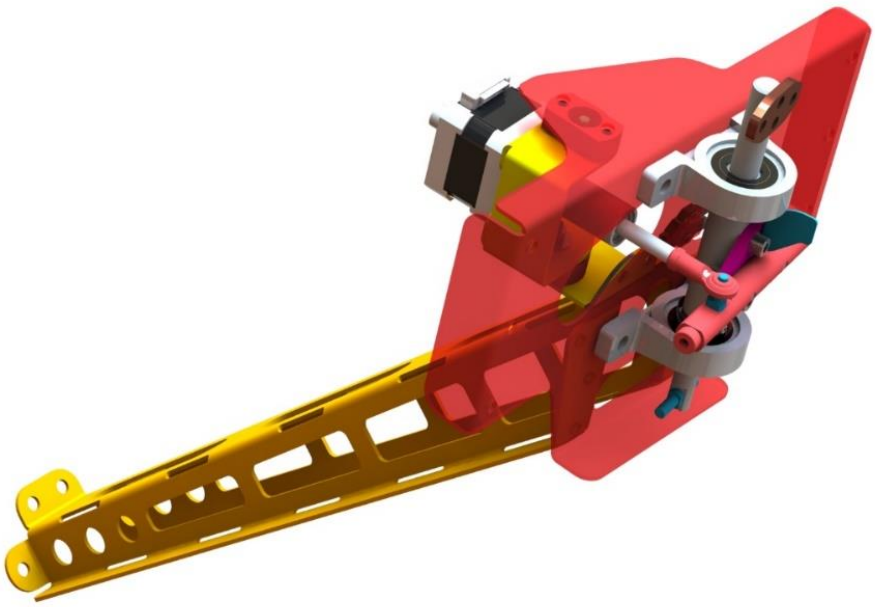

Figure 57. CAD model of the head mechanism.

The mechanism has two degrees of freedom for motion in horizontal and vertical planes. The motion in vertical plane was considered previously and now the horizontal motion will be discussed. This motion is provided by another linear captive actuator which parameters

are shown in table 10. This actuator has the same connection principle as the vertical actuator. A yellow hinge is mounted on bearings with housings, so the actuator can freely rotate in the horizonal plane if it is not fixed. All the force is also transmitted via spherical plane bearing.

Table 10. LGA421S14-B-TJBA-038 captive linear actuator parameters

Max. axial force	*470 N*
Stroke	*38 mm*
Speed	*26 mm/s*
Resolution	*0.005 mm/step*
Max. power output	*3 W*

The actuator is equipped with incremental encoder and the head mechanism has a limiter switch for its calibration. This actuator has power output of only *3 W*, however this is enough, since the actuator works only against static load of *300 N* provided by a rider.

Main parts of the head mechanism are two sheet metal bended plates with *2 mm* thickness. The red plate is used to connect other parts of the assembly and the orange long part transmits force from harness to the rest of the mechanism. It was essential to reduce mass of the head as much as possible as it would drastically decrease bending torque caused by gravitational forces. That is why the orange part has that many slots and holes.

To make the simulator look more realistic a horse head is installed on the head mechanism. The head has only esthetic function and is not involved into mechanism functioning. The head has complex shape and thus it is going to be manufactured with use of additive technologies. Since the head does not withstand heavy loads and high surface quality is not essential, it can be manufactured by FDM (fused deposition modeling) method. Although this manufacturing type does not provide high accuracy and it requires postprocessing, it is cost effective and it allows to print large-scale parts, what makes it the most suitable option in this case.

As the head length is over *700 mm* and its width and height reach almost *400 mm*, it was decided to separate head into several pieces. This will simplify manufacturing process and

allow to use a broad range of FDM printers for manufacturing. The design head parts are shown in figure 58.

Figure 58. Simulator head in assembly and separated.

The head is made hollow for mass and cost reduction. Inside of the head the beam passes to which the end part of the head is bolted. This beam transmits all forces and the simulator head is only loaded with gravitational forces. The only loaded part of the head is flange that is shown in the middle of the figure. The flange is attached to the red plate shown previously and then other head parts are fixed to the flange. Neck artificial skin is also attached to the flange and therefore it is also loaded with tension cased by skin stretching. Intermediate parts of the head have several holes for wires that come from sensors. Head parts will be manufactured from ABS plastic as it is widespread and has sufficient durability and lifetime properties.

Even though the dynamic analysis was carried out, it is not clear if the assembly will be able to withstand external and internal forces. That is why strength calculations of the main parts were made, and the results showed that the connection rod was the most loaded part in the "3-Joint" mechanism. The results are reasonable since the connection rod transmits all the forces from both crankshafts to the head and thus its durability was questionable. Therefore,

it was decided to redesign the connection rod and re-check its strength properties using FEM (finite element method). The improved design is shown in figure 59.

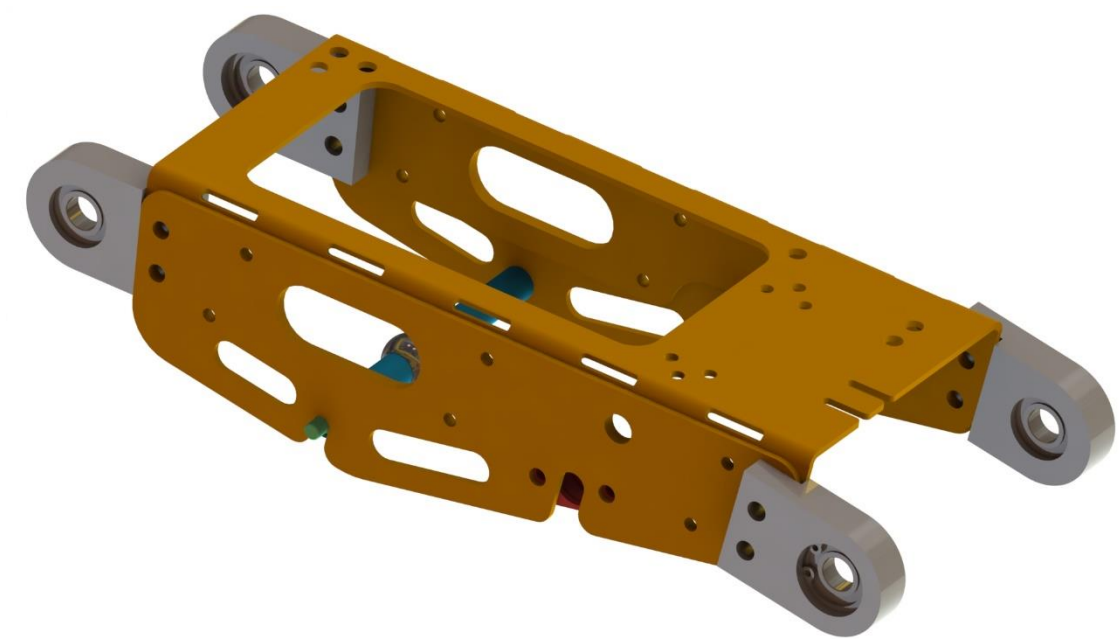

Figure 59. Redesigned connection rod for "3-Joint" mechanism.

The main part of the connection rod is now bended steel plate which is wider and higher that the steel rectangular beam used previously. The dimensions were increased to increase section modulus, and thus, increase overall strength. Even though the part is bigger now its weight has not changed much due to adding of extra slits. The slits are located at the middle of each edge and consequently they do not affect much on the part strength, yet, they help to reduce total mass.

In order to make sure that the new design can withstand all the loads a FEM was used. Bearings at the left side of connection rod were fixed with use of "Joint connection" and the same fixture type was used at the connection with the plain bearing. The distant load was applied to the opposite bearings. The amplitude of the load includes not only gravitational forces that equal to *50 N*, but also include impact from a rider pulling a horse harness with force of *300 N*. All the sheet metal parts are made from 1.0038 low carbon steel. Bearing housings are made from 2024-T3. The setup is shown in figure 60.

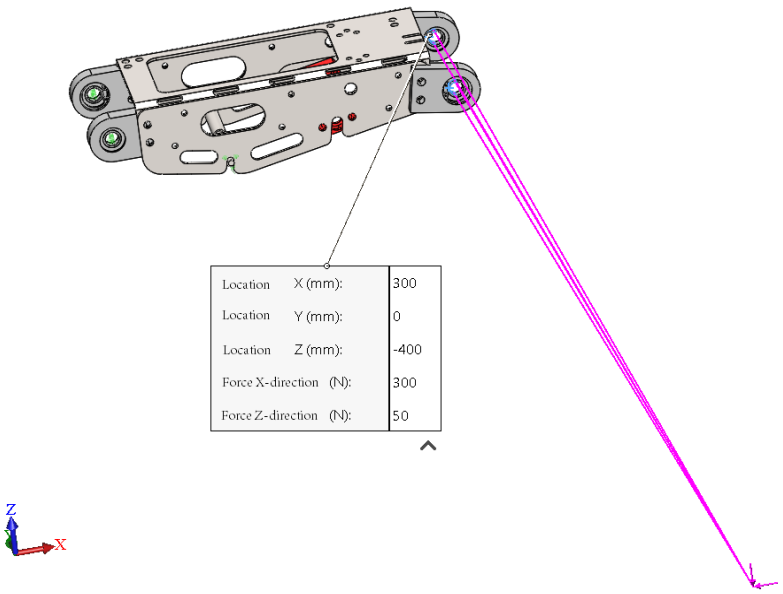

Figure 60. Connection rod FEM setup.

After defining all necessary parameters, a mesh was created, and analysis was carried out. The outcome is shown in figure 60.

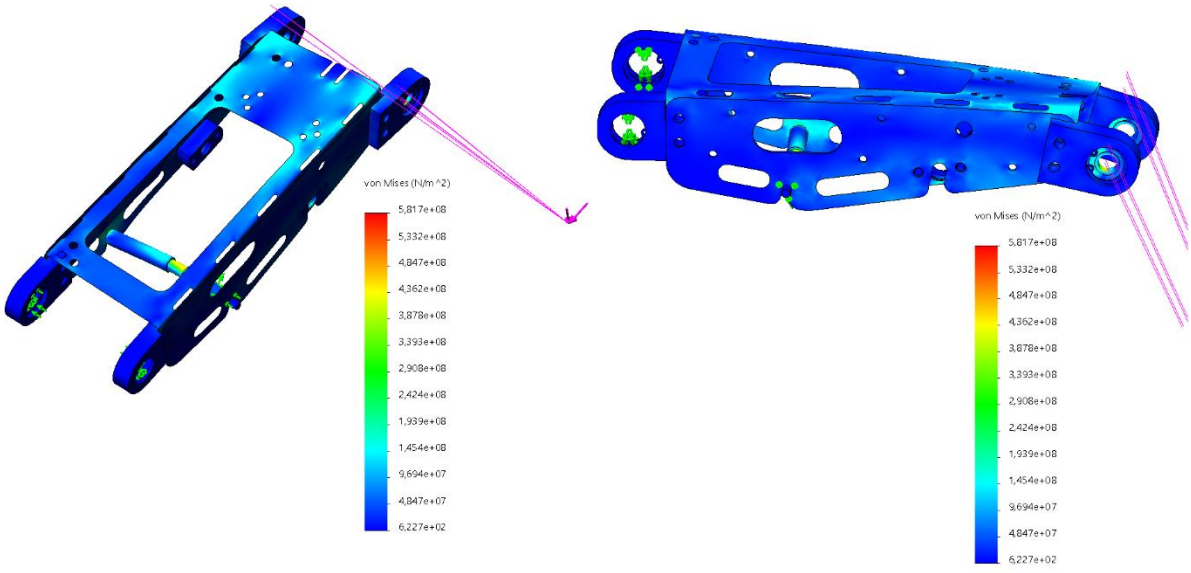

Figure 61. Connection rod FEM results.

The analysis shows that the yield strength is not reached at any part of the rod. The highest stresses are located on a surface of a shaft to which plain bearing will be connected. As this bearing is not a part of the connection rod subassembly, it was not included in the analysis

and, consequently, in reality, the total stresses will be even lower. The other parts of the connection rod are subjected to the maximum stresses of *150 MPa* and thus they can easily withstand cyclic loads.

3 RESULTS

Based on methods discussed previously a complete mechanical design of the horse simulator head and neck mechanism was made. This new mechanism has several improvements in comparison with existing analogues: it has additional degrees of freedom; according to the motion analysis results it recreate more realistic motion and lastly, it has stretchable neck skin that is also makes simulator more similar to a real horse. The final CAD model of the head and neck mechanism is shown in figure 62.

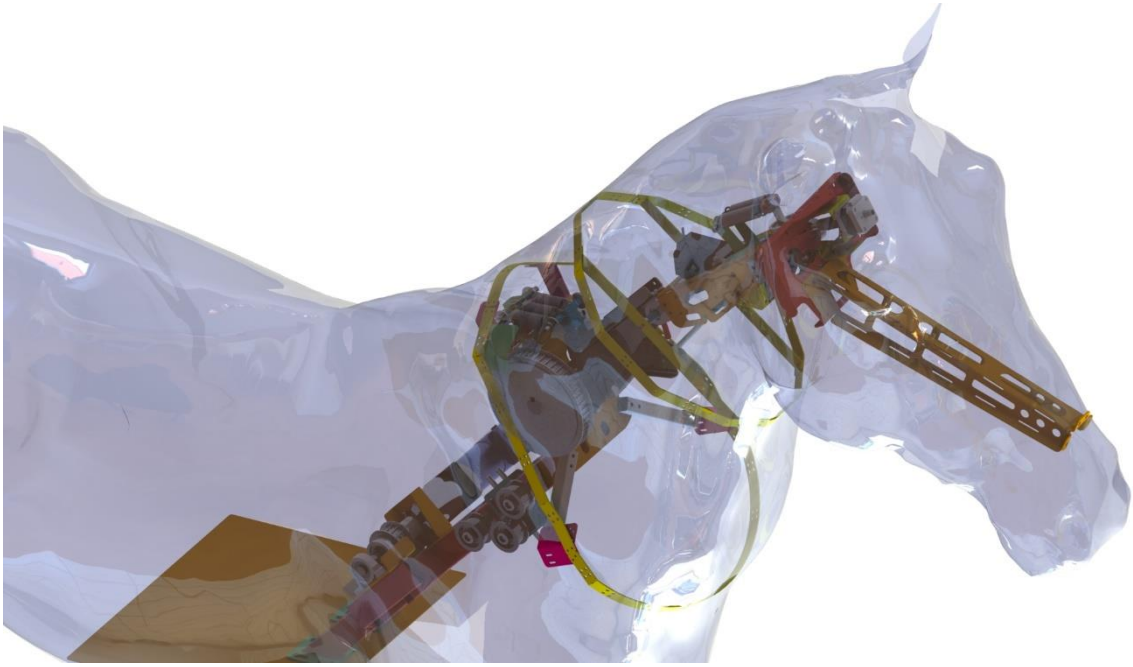

Figure 62. Horse head and neck mechanism final CAD model.

It was important to optimize consumed power, so that more cost-effective actuators could be used. Dynamic modeling has helped to implement this optimization and initial power consumption of *180 W* for neck and *45 W* for head was reduced to only *70 W* for neck and *12 W* for head. Totally the power consumption was reduced in more than *2,5* times. This allowed to reduce cost of the actuators and other drivetrain elements.

Horse head and neck mechanism has a wide range of motion, it is possible not only to recreate walk, trot, and canter gaits, but also to make other natural horse motions. Without

artificial limitations horse head could touch the body of the simulator. Horse head and neck mechanism at its lowest position is shown in figure 63.

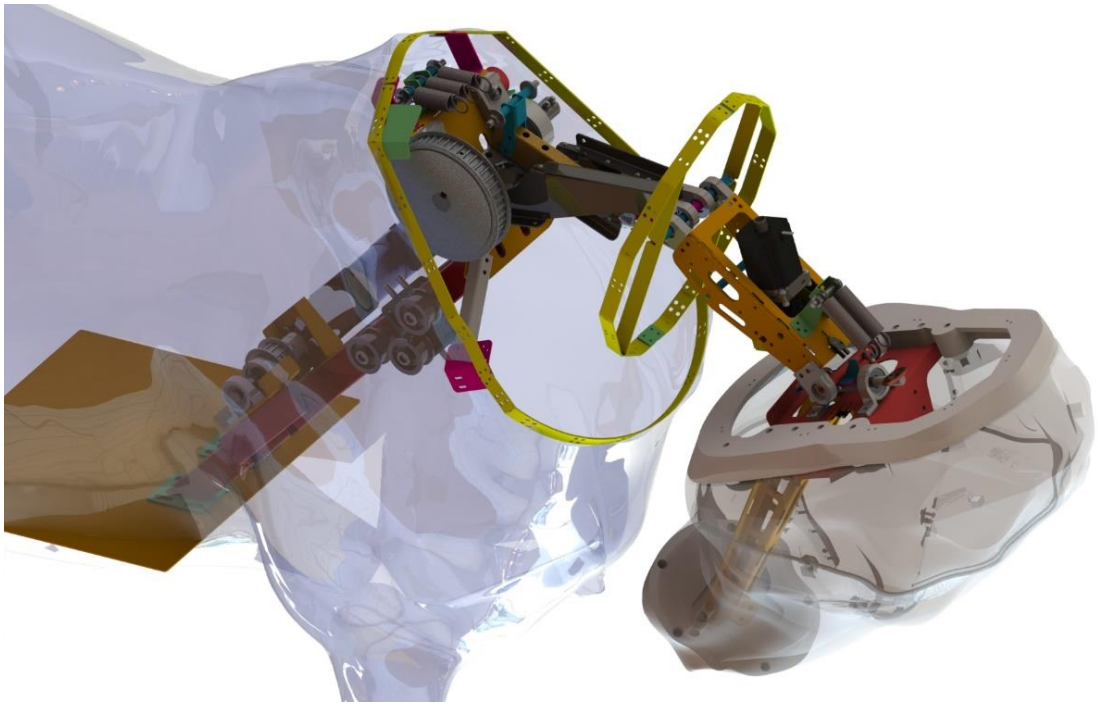

Figure 63. Horse head and neck mechanism CAD model at its lowest position.

Stretchable skin is hard to implement in CAD modeling and since there is no necessity for that it is not shown in the figure. Nevertheless, this skin type is a new feature that has not been used on mass produced horse simulators before. Simulator skin motion similar to a real one will help to immerse equestrian into horse riding and will bring more realistic experience.

4 CONCLUSION

Main tasks of the research were to determine horse head and neck motion patterns and to design a mechanism that could reproduce these patterns. The outcome of the project is the CAD model and drawings that will be used for horse head and neck mechanism manufacturing. Achieved results required accomplishment of different steps that in their turn required multidisciplinary knowledge.

The development process started from motion analysis. Motion capture data and researches were considered to achieve a decent result. The analysis was carried out manually without using software that would analyze data automatically as the manual work provided rapid output.

Mechanism kinematic synthesis that is based on motion analysis was also created manually. The reason for that is current software development level. Nowadays it is possible to automatically generate a mechanism based on desired trajectory, however software discussed in the beginning does not take into account mechanical limitations, it has minor component library and only few dynamic parameters are considered. Thus, a manual synthesis will benefit in a more efficient solution, yet it requires deeper understanding of kinematics and mechanics in general.

For the same reasons during dynamics optimization no software except for Matlab Simscape was used. A software can help with optimization of certain parameters; however, it cannot improve mechanical concept itself and will not come up with a completely new mechanical structure. In the future this fact may change, but currently even manual optimization can increase power efficiency in more than *2,5* times as it was shown in the work. The drawback of this approach is its time consumption. With desire in optimization this process becomes iterative and therefore conclusions made on the last step may require modifications in the first step and all the work must be redone again, sometimes more than once.

Final step is CAD modeling and drawings creation. This part was the most time consuming since it was an iterative process itself. Several mechanical design concepts were tested and

the most suitable from the perspective of desired outcome and manufacturing cost was chosen. Not all minor steps were discussed in the work such as parts and assembly drawings or some tested mechanical concepts that turned out to be inefficient.

The main focus in this work was to reproduce horse head and neck realistic motion pattern. This motion should feel realistic for a horse rider and thus to check the achieved result it must be tested by equestrian experts. As head and neck move independently it is possible to make software adjustments to improve motion patter. This validation and improvement process will take place in the future after the mechanism will be assembled.

LIST OF REFERENCES

Artas Engineering Software. 2019. SAM Mechanism design. [Artas Engineering Software webpage]. Updated August 26, 2019. [Referred 03.5.2020]. Available: https://www.artas.nl/en/

Bhatti, Z., Shah, A. & Shahidi, F. 2013. Procedural Model of Horse Simulation. 12th ACM SIGGRAPH International Conference on Virtual-Reality. 139-146. 10.1145/2534329.2534364.

Cabibihan, J., Pattofatto, S., Jomaa, M., Benallal, A., & Carrozza, M. 2009. Towards Humanlike Social Touch for Sociable Robotics and Prosthetics: Comparisons on the Compliance, Conformance and Hysteresis of Synthetic and Human Fingertip Skins. International Journal of Social Robotics. 20 p.

COMPMECH Research Group. 2020. GIM Software. [Compmech Research Group webpage]. Updated January 1, 2020. [Referred 02.5.2020]. Available: http://www.ehu.eus/compmech/software/

Guangzhou Steki Amusement Equipment Co., Ltd. 2020. VR Horse. [Guangzhou Steki Amusement Equipment Co., Ltd webpage]. Updated May 11, 2020. [Referred 26.4.2020]. Available: https://www.stekiamusement.com/vr-war-horse-simulator/

Ha, S., Coros, S., Alspach, A., Bern, J., Kim, J. & Yamane, K. 2018. Computational Design of Robotic Devices From High-Level Motion Specifications. IEEE Transactions on Robotics. PP. 1-12. 10.1109/TRO.2018.2830419.

Loscher, D., Meyer, F., Kracht, K. & Nyakatura, J. 2016. Timing of head movements is consistent with energy minimization in walking ungulates. Royal Society B: Biological Sciences. 283. 10.1098/rspb.2016.1908.

Padilha, F., Andrade, A., Fonseca, A., Godoi, F., Almeida, F. & Ferreira, A. 2017. Morphometric measurements and animal-performance indices in a study of racial forms of Brazilian Sport Horses undergoing training for eventing. Revista Brasileira de Zootecnia. 46. 25-32. 10.1590/s1806-92902017000100005.

Pat. US 20110087354A1. 2016. Modeling skin-covered robotics devices including artistic digital iterative design processes. Disney Enterprises Inc. (Bryan S. TyePhilip John Jackson) Appl. US12/971,317, 2010-12-17. Publ. 2016-08-02. 41 p.

Pat. US 7749088B2. 2010. Horse simulator. Racewood Ltd. (William Ronald Greenwood) Appl. US12/073,900, 2008-03-11. Publ. 2010-07-06. 8 p.

Racewood Ltd. 2020. Racewood horse-riding simulator. [Racewood Ltd webpage]. Updated April 28, 2020. [Referred 15.3.2020]. Available https://www.racewood.com/pictures.html

Rhodin, M. 2008. A Biomechanical Analysis of Relationship Between the Head and Neck Position, Vertebral Column and Limbs in the Horse at Walk and Trot. Doctoral thesis. Swedish University of Agricultural Sciences. 72 p.

Tan, N., Sun, Z., Mohan, R., Brahmananthan, N., Venkataraman, S., Sosa, R. & Wood, K. 2019. A System-of-Systems Bio-Inspired Design Process: Conceptual Design and Physical Prototype of a Reconfigurable Robot Capable of Multi-Modal Locomotion. Front. Neurorobot. 13:78. doi: 10.3389/fnbot.2019.00078

Torres-Pérez, Y., Gómez-Pachón, E., & Cuenca-Jiménez, F. 2016. Horse´s gait motion analysis system based on videometry. Ciencia Y Agricultura, 13(2), 83-94.

Wilhelm, N., Vögele, A., Zsoldos, R., Licka T., Krüger, B. & Bernard, J. 2015. FuryExplorer: Visual-Interactive Exploration of Horse Motion Capture Data. Proceedings of SPIE - The International Society for Optical Engineering. 16 p.